

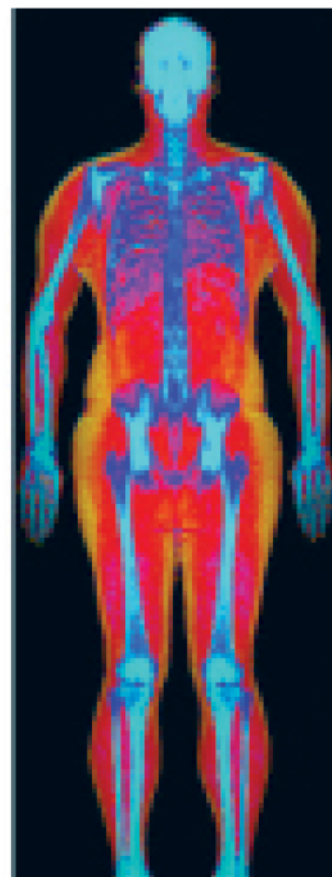
Powerful images. Clear answers.



Manage Patient's concerns about
Atypical Femur Fracture*



Vertebral Fracture Assessment –
a critical part of a complete
fracture risk assessment



Advanced Body Composition®
Assessment – the power to
see what's inside

Contact your Hologic rep today at BSHSalesSupportUS@hologic.com







PAID ADVERTISEMENT

*Incomplete Atypical Femur Fractures imaged with a Hologic densitometer, courtesy of Prof. Cheung, University of Toronto

ADS-02018 Rev 003 (10/19) Hologic Inc. ©2019 All rights reserved. Hologic, Advanced Body Composition, The Science of Sure and associated logos are trademarks and/or registered trademarks of Hologic, Inc., and/or its subsidiaries in the United States and/or other countries. This information is intended for medical professionals in the U.S. and other markets and is not intended as a product solicitation or promotion where such activities are prohibited. Because Hologic materials are distributed through websites, eBroadcasts and tradeshows, it is not always possible to control where such materials appear. For specific information on what products are available for sale in a particular country, please contact your local Hologic representative.

www.hologic.com | dxaperformance.com | 1.800.442.9892

Piezo1 Inactivation in Chondrocytes Impairs Trabecular Bone Formation

Gretl Hendrickx,¹  Verena Fischer,²  Astrid Liedert,² Simon von Kroge,¹ Melanie Haffner-Luntzer,² Laura Brylka,¹  Eva Pawlus,¹ Michaela Schweizer,³ Timur Yorgan,¹  Anke Baranowsky,¹ Tim Rolvien,¹ Mona Neven,¹ Udo Schumacher,⁴ David J Beech,⁵ Michael Amling,¹  Anita Ignatius,^{2*} and Thorsten Schinke^{1*} 

¹Department of Osteology and Biomechanics, University Medical Center Hamburg-Eppendorf, Hamburg, Germany

²Institute of Orthopedic Research and Biomechanics, University Medical Center Ulm, Ulm, Germany

³Department of Electron Microscopy, Center of Molecular Neurobiology, University Medical Center Hamburg-Eppendorf, Hamburg, Germany

⁴Institute of Anatomy and Experimental Morphology, University Cancer Center, University Medical Center Hamburg-Eppendorf, Hamburg, Germany

⁵Leeds Institute of Cardiovascular and Metabolic Medicine, School of Medicine, University of Leeds, Leeds, UK

ABSTRACT

The skeleton is a dynamic tissue continuously adapting to mechanical stimuli. Although matrix-embedded osteocytes are considered as the key mechanoresponsive bone cells, all other skeletal cell types are principally exposed to macroenvironmental and microenvironmental mechanical influences that could potentially affect their activities. It was recently reported that Piezo1, one of the two mechanically activated ion channels of the Piezo family, functions as a mechanosensor in osteoblasts and osteocytes. Here we show that Piezo1 additionally plays a critical role in the process of endochondral bone formation. More specifically, by targeted deletion of *Piezo1* or *Piezo2* in either osteoblast (*Runx2Cre*) or osteoclast lineage cells (*Lyz2Cre*), we observed severe osteoporosis with numerous spontaneous fractures specifically in *Piezo1^{Runx2Cre}* mice. This phenotype developed at an early postnatal stage and primarily affected the formation of the secondary spongiosa. The presumptive *Piezo1^{Runx2Cre}* osteoblasts in this region displayed an unusual flattened appearance and were positive for type X collagen. Moreover, transcriptome analyses of primary osteoblasts identified an unexpected induction of chondrocyte-related genes in *Piezo1^{Runx2Cre}* cultures. Because *Runx2* is not only expressed in osteoblast progenitor cells, but also in pre-hypertrophic chondrocytes, these data suggested that Piezo1 functions in growth plate chondrocytes to ensure trabecular bone formation in the process of endochondral ossification. To confirm this hypothesis, we generated mice with *Piezo1* deletion in chondrocytes (*Col2a1Cre*). These mice essentially recapitulated the phenotype of *Piezo1^{Runx2Cre}* animals, because they displayed early-onset osteoporosis with multiple fractures, as well as impaired formation of the secondary spongiosa with abnormal osteoblast morphology. Our data identify a previously unrecognized key function of Piezo1 in endochondral ossification, which, together with its role in bone remodeling, suggests that Piezo1 represents an attractive target for the treatment of skeletal disorders. © 2020 The Authors. *Journal of Bone and Mineral Research* published by Wiley Periodicals LLC on behalf of American Society for Bone and Mineral Research (ASBMR).

KEY WORDS: CHONDROCYTE; ENDOCHONDRAL OSSIFICATION; MECHANOSENSATION; OSTEOBLAST; PIEZO1

Introduction

Skeletal development, growth, and remodeling are highly complex processes involving many different cell types with unique functions.⁽¹⁾ Whereas a small subset of skeletal elements, mostly in the skull, develops by intramembranous ossification, where mesenchymal progenitor cells directly differentiate into bone-forming osteoblasts, the majority of the axial and

appendicular skeleton develops by endochondral ossification.^(2,3) In this latter process the mesenchymal progenitor cells initially condensate into cell clusters which differentiate into chondrocytes to produce a cartilage intermediate that is subsequently replaced by bone. At the end of puberty, this modeling phase is essentially replaced by bone remodeling, a physiologically relevant process, which is mediated by the coordinated

This is an open access article under the terms of the Creative Commons Attribution License, which permits use, distribution and reproduction in any medium, provided the original work is properly cited.

Received in original form May 8, 2020; revised form September 21, 2020; accepted October 11, 2020.

Address correspondence to: Thorsten Schinke, PhD, Department of Osteology and Biomechanics, University Medical Center Hamburg Eppendorf, Martinistrasse 52, Hamburg 20246, Germany. E-mail: schinke@uke.de

Additional Supporting Information may be found in the online version of this article.

*These authors contributed equally to this work.

Journal of Bone and Mineral Research, Vol. 00, No. 00, Month 2020, pp 1–16.

DOI: 10.1002/jbmr.4198

© 2020 The Authors. *Journal of Bone and Mineral Research* published by Wiley Periodicals LLC on behalf of American Society for Bone and Mineral Research (ASBMR).

activities of bone-resorbing osteoclasts and osteoblasts.⁽⁴⁾ The rate of bone remodeling is controlled, at least in part, by osteocytes, representing terminally differentiated osteoblasts forming an extensive cellular network within the mineralized bone matrix.⁽⁵⁾ Bone remodeling is strongly influenced by mechanical loading, which is most evident in astronauts, who lose as much as 2% of their bone mass each month when exposed to microgravity, or in professional tennis players, who have up to 35% more bone in their serving arm as in their contralateral arm.^(6–8) Moreover, absence of mechanical stimuli (eg, chronic bed rest or low physical activity) negatively affects skeletal integrity in the general population.

In this context osteocytes are considered the primary mechanosensing cell type of the skeleton, because they can sense mechanical stimuli and react by differential expression of genes affecting bone remodeling.^(9,10) Importantly, however, osteocytes are probably not the only skeletal cell types experiencing mechanical forces. In fact, there is increasing evidence for an impact of mechanobiology on various cells involved in developmental and regenerative processes, and it is likely that the cellular processes required for bone elongation are also controlled by mechanical forces.^(11,12) More specifically, longitudinal bone growth depends on growth plate chondrocytes that undergo a complex multistep differentiation process, which takes place in a nonvascularized rigid extracellular matrix. After distinct morphological changes, these cells become hypertrophic and eventually produce a calcified cartilage matrix, which serves as a scaffold for trabecular bone formation.^(13,14) This region, termed primary spongiosa, is subsequently replaced by bone through the concerted action of osteoclasts and osteoblasts, which leads to the formation of trabecular bone below the growth plates that is the secondary spongiosa. Importantly, whereas the hematopoietic osteoclast progenitors enter the primary and secondary spongiosa through the vasculature, there is increasing evidence for the necessity of chondrocyte-to-osteoblast transdifferentiation to generate the osteoblasts required for trabecular bone formation.^(15,16)

To understand the molecular bases of skeletal mechanosensation, we and others aimed at identifying specific proteins, which are expressed by skeletal cells to sense mechanical forces and to translate them into a biological response. Based on accumulating evidence from nonskeletal cell types, there were two excellent candidates to mediate mechanosensation in the skeleton, ie, the members of the Piezo family, which were identified 10 years ago as mechanically activated ion channels.⁽¹⁷⁾ Both Piezo1 and Piezo2 represent large transmembrane proteins with the ability to homomultimerize, and their unique and huge transmembrane channel structure enables them to be activated by stretching of cell membranes.^(18–20) Because Piezo channels are broadly expressed, it is not surprising that their impact on mechanotransduction has been shown for a variety of different cellular processes. For Piezo1 it was reported that its expression is required for the alignment of endothelial cells along the direction of blood flow, for the control of epithelial cell numbers through sensing of either mechanical crowding or stretch, or for the response of innate immune cells to hydrostatic pressure in the lung.^(21–23) In contrast, Piezo2 was reported to play a major role in Merkel cells and sensory neurons of the skin, and as an airway stretch mechanosensor in the lung.^(24–26) Whereas the majority of these findings were obtained in mouse models, *PIEZO* mutations have also been found to cause specific human disorders. More specifically, *PIEZO1* mutations were identified as a cause of dehydrated hereditary stomatocytosis (gain-of-function) or lymphatic malformation (loss-of-function),

whereas *PIEZO2* mutations were found to cause Marden-Walker syndrome (MWS) or distal arthrogryposis.^(27–31)

The first evidence for an impact of Piezo proteins on the skeleton was reported in 2019, where *PIEZO1* was identified as a genetic determinant of estimated bone mineral density in humans.⁽³²⁾ More recently, murine Piezo1 was identified to be required for mechanosensation by osteoblasts at different stages of differentiation, where it mediates the osteoanabolic influence of mechanical loading and controls the crosstalk between osteoblasts and osteoclasts.^(33–35) Most recently, it was additionally reported that the combined inactivation of Piezo1 and Piezo2 in limb mesenchymal cells causes severe osteoporosis with accompanying fractures in the appendicular skeleton of neonatal mice.⁽³⁶⁾ Although these findings, all reported during the time of our own analyses, clearly demonstrated a key role of Piezo1 for skeletal integrity, there were still many open questions that remain to be addressed. For instance, the role of Piezo2 in the different skeletal cell types has not been systematically studied. Moreover, because a function of Piezo1 in osteoblast progenitors was uncovered by the use of *Prx1Cre* mice, an impact on the axial skeleton could not be analyzed here. Finally, and most importantly, it has not been addressed so far, if the influence of Piezo1 on endochondral ossification depends on its expression in chondrocytes.

Here we describe a systematic analysis of mouse models lacking Piezo1 and/or Piezo2 in different skeletal cell types. We thereby confirmed that Piezo1 is required for mechanosensation by osteocytes, and we additionally demonstrate a previously unrecognized function of Piezo1 in growth plate chondrocytes, which is required for trabecular bone acquisition. Our data complement the previous studies involving other mouse lines to provide a near complete knowledge on the key functions of Piezo proteins in skeletal development, growth, and remodeling.

Materials and Methods

Cell culture

Primary osteoblasts were isolated by sequential collagenase-dispase II digestion from the calvariae of 5-day-old mice and differentiated in the presence of α -Minimum Essential Medium Eagle (α -MEM; Sigma-Aldrich, St. Louis, MO, USA) supplemented with 10% FCS (Hyclone Laboratories, Logan, UT, USA), 1% Pen/Strep (Gibco, Grand Island, NY, USA), 50 μ g/mL ascorbic acid and 10mM β -glycerophosphate as described.⁽³⁷⁾ After 2 days of differentiation, cells were serum-starved overnight and then treated for 6 hours with Yoda1 (5 μ M; Tocris Bioscience, Bristol, UK; 5586). For the generation of primary osteoclasts, bone marrow was flushed out of the femurs from 12-week-old mice. Cells were then cultured α -MEM (10% FBS [Gibco], 1% Pen/Strep) supplemented with 10nM 1,25-dihydroxyvitamin-D3. At day 4 after seeding, M-CSF (PeproTech, Rocky Hill, NJ, USA; 315-02) and sRANK Ligand (PeproTech; 315-11) were added to a final concentration of 20 and 40 ng/mL, respectively. Mouse preosteoblastic calvarial MC3T3-E1 cells (CRL-2593; American Type Culture Collection (ATCC), Manassas, VA, USA) were cultured in α -MEM (Lonza, Basel, Switzerland; BE12-169F) supplemented with 10% FCS (Merck Millipore, Burlington, MA, USA; S0605) and incubated in 5% CO₂ and at 37°C. Chondrogenic ATDC5 cells (Sigma-Aldrich; 99072806) were grown in Dulbecco's Modified Eagle Medium/Ham's F12 Nutrient mixture (DMEM/F12; Thermo Fisher Scientific, Waltham, MA, USA; 21331-020) supplemented with 5% FCS, 10 μ g/mL transferrin (Sigma-Aldrich; T8158), and 30nM sodium selenite (Sigma-Aldrich; S5261).

Expression analysis

RNA was isolated using the RNeasyMini kit (QIAGEN, Valencia, CA, USA), and DNase I digestion was performed according to the manufacturer's instructions. Concentration and quality of RNA were measured using a NanoDrop ND-1000 system (NanoDrop, Thermo Fisher Scientific, Waltham, MA, USA) and the TapeStation 2200 system (Agilent Technologies, Santa Clara, CA, USA). For genome-wide expression analysis, 100 ng of total RNA were used for the synthesis of proprietary labeled 2nd-cycle single-stranded complementary DNA (ss-cDNA) utilizing the Clariom D assay, mouse (Thermo Fisher Scientific). Samples were prepared according to the manufacturer's GeneChip™ WT PLUS reagent kit manual (document 703174; revision A.0). For Gene Chip hybridization, 5.5 µg of fragmented and labeled cDNA was incubated in hybridization solution at 45°C for 16 hours, before the Gene Chips (Clariom D, mouse) were washed using the Affymetrix Fluidics Station 450 (Affymetrix, Santa Clara, CA, USA). Microarrays were scanned with the Affymetrix Gene Chip Scanner 7G, and the signals were analyzed with the Transcriptome Analysis Console software (TAC 4.0; Thermo Fisher Scientific) using default analysis settings (version 1) and Gene + Exon – signal space transformation–robust multiarray analysis (SST-RMA) as summarization. The gene expression data have been deposited at the GEO database (National Center for Biotechnology Information [NCBI], Bethesda, MD, USA; <https://www.ncbi.nlm.nih.gov/geo/>) with accession number GSE138159 (primary osteoblasts) and GSE138160 (MC3T3-E1 cells). For qRT-PCR expression analysis, 1 µg of RNA was reversed transcribed using Verso cDNA Synthesis Kit (Thermo Fisher Scientific) according to the manufacturer's instructions. Quantitative expression analysis was performed using a StepOnePlus system and predesigned TaqMan gene expression assays (Applied Biosystems, Foster City, CA, USA). *Gapdh* expression was used as an internal control. Relative quantification was performed according to the comparative threshold cycle ($\Delta\Delta CT$) method, and results were expressed in the linear form using the delta-delta comparative threshold cycle formula ($2^{-\Delta\Delta CT}$).

Mechanical loading experiments in vitro

MC3T3-E1 cells were plated at a density of 10,000 cells/cm² on collagen-coated glass slides (Flexcell, Burlington, NC, USA; CS-C). Cells were subjected or not subjected (static control) to mechanical stimulation by laminar fluid flow (LFF) with a shear stress of 10 dynes/cm² for 1 hour using the Streamer System (FlexCell; STR-4000). RNA samples were obtained immediately (0 hours), 2 and 4 hours after LFF.

RNA interference and treatment with Yoda1

MC3T3-E1 cells were seeded at a density of 10,000 cells/cm² on collagen-coated glass slides (FlexCell; CS-C). Silencer Select Piezo1 siRNA (Thermo Fisher Scientific; s107968) or Silencer Negative Control siRNA (Thermo Fisher Scientific; AM4636) was added at a concentration of 5 pmol/µL to the cells in serum-reduced (1% FCS) α -MEM without antibiotics using Lipofectamine (Thermo Fisher Scientific; 13778030) in Opti-MEM (Thermo Fisher Scientific; 31985062) for transfection. Cells were incubated in 5% CO₂ at 37°C for 48 hours before LFF was applied. Treatment with Yoda1 (5 µM) was performed in serum-reduced (1% FCS) α -MEM for 6 hours. DMSO vehicle was used at a concentration of 0.01% as control.

Mouse models

Generation and genotyping *Piezo1*^{fl/fl} and *Piezo2*^{fl/fl} mice (the latter ones kindly provided by A. Patapoutian The Scripps

Research Institute, La Jolla, CA, USA.) have been described previously.^(22,26) The same applies for the four *Cre*-expressing mouse lines that were used in this study.^(38–41) Whereas *Lyz2Cre* (#004781), *Dmp1Cre* (#023047), and *Col2a1Cre* (#003554) mice were obtained by the The Jackson Laboratory (Bar Harbor, ME, USA), *Runx2Cre* mice were kindly provided by J. Tuckermann (Ulm University, Ulm, Germany). To rule out any possible influence of genetic background, all analyses were performed with the corresponding *Cre*-negative littermate controls. Mice were housed in a specific pathogen-free environment with a 12-hour light/dark cycle, 45% to 65% relative humidity and 20°C to 24°C ambient temperature in open or individually ventilated cages with wood shavings bedding and nesting material in groups not surpassing six animals. Mice had *ad libitum* access to tap water and standard rodent chow (1328P; Altromin Spezialfutter GmbH & Co. KG, Lage, Germany). Animal care and all experimental procedures were performed with approval from the animal care committees of the University Medical Center Hamburg-Eppendorf (N18/073, Org869).

Ex vivo calibration and mechanical loading in vivo

The mechanical loading regime was calibrated as described.⁽⁴²⁾ Briefly, strain gauges were applied to the lateral medial surface of the ulnas of 12-week-old female *Piezo1*^{fl} (*n* = 6) and *Piezo1-Dmp1Cre* (*n* = 6) mice postmortem. The right ulna was positioned in the loading apparatus and the load required to produce a peak surface strain of 2000 microstrain (µstrain) during locomotion were recorded. Generated strains were different between the genotypes, wherefore cyclic axial compression of the right ulna was performed using a frequency of 2 Hz and a maximum load of 1.5 N and 0.62 N in 12-week-old female *Piezo1*^{fl} and *Piezo1-Dmp1Cre* mice, respectively. After ex vivo calibration, in vivo loading was performed on ulnas of 12-week-old female *Piezo1*^{fl} (*n* = 6) and *Piezo1-Dmp1Cre* (*n* = 6) mice during anesthesia on three consecutive days for 1 min each. The left ulnas were used as nonloaded controls. All mice received a subcutaneous injection of Calcein green (0.03 g/kg) on day 3 and Alizarin red (0.045 g/kg) on day 12 and were euthanized on day 16. Animals were allocated to the different groups based on their genotype. Because of the different maximum loads for each genotype, investigators were not blinded during the allocation and animal handling. Blinding was given for endpoint measurements after the animals were euthanized. No adverse events were observed. These experimental procedures were performed with approval from the animal care committee of Baden-Württemberg (Regierungspräsidium Tübingen, No. 1388).

Micro-computed tomography and histomorphometry of ulnas

Ulnas were scanned using a micro-computed tomography (µCT) device (Skyscan 1172; Bruker, Kontich, Belgium) as described (8 µm, 50 kV, 200 mA, hydroxyapatite phantoms: 250 and 750 mg hydroxyapatite [HA]/cm³).⁽⁴³⁾ A 1-mm-thick section of the mid-diaphyseal cortical bone, beginning 3 mm distally from the ulna head, was analyzed as region of interest. Using a fluorescent microscope (Leica, Wetzlar, Germany; DMI6000 B), periosteal bone formation rate (BFR/BS) was determined in 10-µm-thick cross-sections of the left and right ulnas using image analysis software (Leica; MMAF 1.4.0) with an interlabel time (Ir.L.t) of 9 days. BFR was calculated as described.⁽⁴²⁾

Skeletal phenotyping

Dissected skeletons were fixed in 3.7% PBS-buffered formaldehyde for 18 hours, before they were stored in 80% ethanol. After initial assessment by contact X-ray, the lumbar vertebral bodies L₁ to L₄ and one tibia were dehydrated in ascending alcohol concentrations and then embedded in methylmethacrylate for undecalcified histology as described.⁽⁴⁴⁾ For μ CT scanning, we used the left femurs that were scanned using a μ CT 40 desktop cone-beam microCT (SCANCO Medical AG, Brüttisellen, Switzerland) with a voxel size of 10 μ m (1000 projections per slice with 2048 samples and 200-s sample time at a tube energy of 55 kVp with an intensity of 145 mA). Reconstructed slices were analyzed using the SCANCO MicroCT software suite. Trabecular bone was analyzed in the distal metaphysis in the region 2.5 to 0.5 mm proximal of the growth plate using the evaluation script 'UCT_EVALUATIONV6_MULTIAUTO'. This script was also used for analysis of cortical bone at the middle of the diaphysis for a length a 1 mm. Pelvis bones were scanned and evaluated utilizing the same protocol with the volume of interest extended to include the whole bone. The pelvic angle was determined on aligned 3D reconstructions. Staining of skeletons with Alcian blue and Alizarin red was performed as described.⁽⁴⁵⁾ To allow quantification of the BFR, all animals received two doses of calcein (30 mg/kg i.p.; Sigma-Aldrich) 10 and 3 days before euthanasia. Histological sections of 4 μ m thickness from the sagittal plane were stained by Toluidine blue, by von Kossa/van Gieson or by Masson-Goldner staining procedures as described.⁽⁴⁴⁾ Histomorphometry was performed according to the ASBMR guidelines using the OsteoMeasure histomorphometry system (OsteoMetrics, Decatur, GA, USA).⁽⁴⁶⁾ Quantification of the osteocyte canalicular network was performed on plastic-embedded tibia specimens by acid etching and subsequent scanning electron microscopy as described.⁽⁴⁷⁾ All quantitative analyses were performed in a blinded fashion. To determine collagen production and processing we measured serum concentrations of procollagen type 1 N propeptide (P1NP) and carboxy-terminal propeptide of type 1 procollagen (P1CP) by ELISA (Cloud-Clone Corp, Houston, TX, USA; Sea957Mu and Sea570Mu).

Immunohistochemistry

For immunohistochemical analysis of collagen type X, dissected skeletons were first fixed in 3.7% PBS-buffered formaldehyde, before they were stored in 80% ethanol, decalcified in EDTA, and embedded in paraffin. Sections of 5 μ m thickness were cut, and after deparaffinization, slides were pretreated with pepsin (S3002; DAKO, Carpinteria, CA, USA) for enzymatic antigen retrieval. Endogenous peroxidase activity was blocked through incubation with 3% H₂O₂ in methanol. Using the DAKO ARK™ (Animal Research Kit, K3954; DAKO), slides were incubated with the primary antibody to collagen type X (2031501001, 1:20; Quartett, Berlin, Germany) overnight at 4°C. Sections were treated with streptavidin-horseradish peroxidase (HRP) and peroxidase activity was visualized using the DAB+ substrate-chromogen solution. Finally, slides were counterstained with hematoxylin and mounted.

In vitro endochondral ossification assay

Chondrogenic ATDC5 cells were seeded at a density of 8000 cells/well in 24-well plates in chondrogenic DMEM/Ham's F12 medium supplemented with 5% FCS, 10 μ g/mL transferrin, 30nM sodium selenite, 0.2mM ascorbate-2-phosphate (Sigma; A8960) and 10 μ g/mL insulin (Sigma; I9278). Cells were

incubated in 6% O₂ at 37°C. At day 7, chondrogenic medium was replaced by osteogenic α -MEM supplemented with 10% FCS, 10mM β -glycerophosphate (Sigma; G5422) 0.2mM ascorbate 2-phosphate, 100 ng/mL recombinant BMP2 (Thermo Fisher Scientific; PHC7145), with or without 5 μ M Yoda1 and cells were cultivated in 21% O₂ at 37°C until day 10. RNA lysates were obtained at days 8, 9, and 10 of cultivation. Alternatively, the same culture conditions were applied with or without addition of 4 μ M GsMTx4 (Abcam, Cambridge, UK; ab141871) to the medium. In another set of experiments, we transfected the cells at day 7 with Silencer Select Piezo1 siRNA or Silencer Negative Control siRNA, as described for MC3T3-E1 cells in the section RNA interference and treatment with Yoda1.

Statistical analysis

All data are presented as box plots, either median with interquartile range where whiskers indicate minimum to maximum or median and minimum to maximum. For the comparison of two groups, statistical analysis was performed using unpaired, two-tailed Student's *t* test. For the comparison of multiple groups, we used ANOVA (Graph Pad Prism; GraphPad Software, Inc., La Jolla, CA, USA). In both cases, *p* values <.05 were considered statistically significant.

Results

Piezo1 activation in osteoblasts induces the expression of mechanoresponsive genes

To uncover a potential impact of Piezo proteins on skeletal cell types, we first analyzed transcription of *Piezo1* and *Piezo2* in different murine tissues and primary bone cells. Whereas *Piezo1* displayed the highest expression in early differentiating osteoblast progenitors (Fig. 1A), *Piezo2* expression was induced during the osteoclastogenic differentiation of bone marrow cells (Fig. 1B). Based on these initial findings, we analyzed the transcriptional response of primary osteoblasts towards the Piezo1-specific agonist Yoda1.⁽⁴⁸⁾ More specifically, we treated three independent sets of primary calvarial osteoblasts at day 2 of osteogenic differentiation with Yoda1 (5 μ M) for 6 hours to identify immediate transcriptional targets by genomewide expression analysis (Fig. 1C,D). Interestingly, two of the most strongly induced genes were *Ptgs2* (encoding cyclooxygenase-2) and *Serpine1*, both known to be transcriptionally activated in bone cells by mechanical loading.⁽⁷⁾ Moreover, a single whole-transcriptome analysis of MC3T3-E1 osteoblasts 0 and 4 hours after mechanical stimulation with LFF also induced *Ptgs2* and *Serpine1* expression (Fig. 1E,F; Supplementary Fig. 1A). We additionally analyzed our data sets regarding the regulation of previously established Piezo1-regulated genes,^(33–35) but here we only observed nonsignificant or very moderate differences (Supplementary Fig. 1B,C).

As confirmed by qRT-PCR, LFF caused a significant induction of *Piezo1* expression in MC3T3-E1 osteoblasts, not immediately, but 2 and 4 hours after mechanostimulation (Fig. 1G). To analyze if Piezo1 activity is required for mechanosensation by osteoblasts, we examined the influences of Yoda1 and LFF on gene expression after application of siRNA-mediated knockdown of *Piezo1* in MC3T3-E1 osteoblasts. We observed that the Yoda1-mediated induction of *Ptgs2* and *Serpine1* was strongly reduced by siRNA-mediated knockdown of *Piezo1*, as expected (Fig. 1H). In contrast, there was only a minor reduction in the LFF-mediated induction of *Serpine1*, whereas *Ptgs2* expression

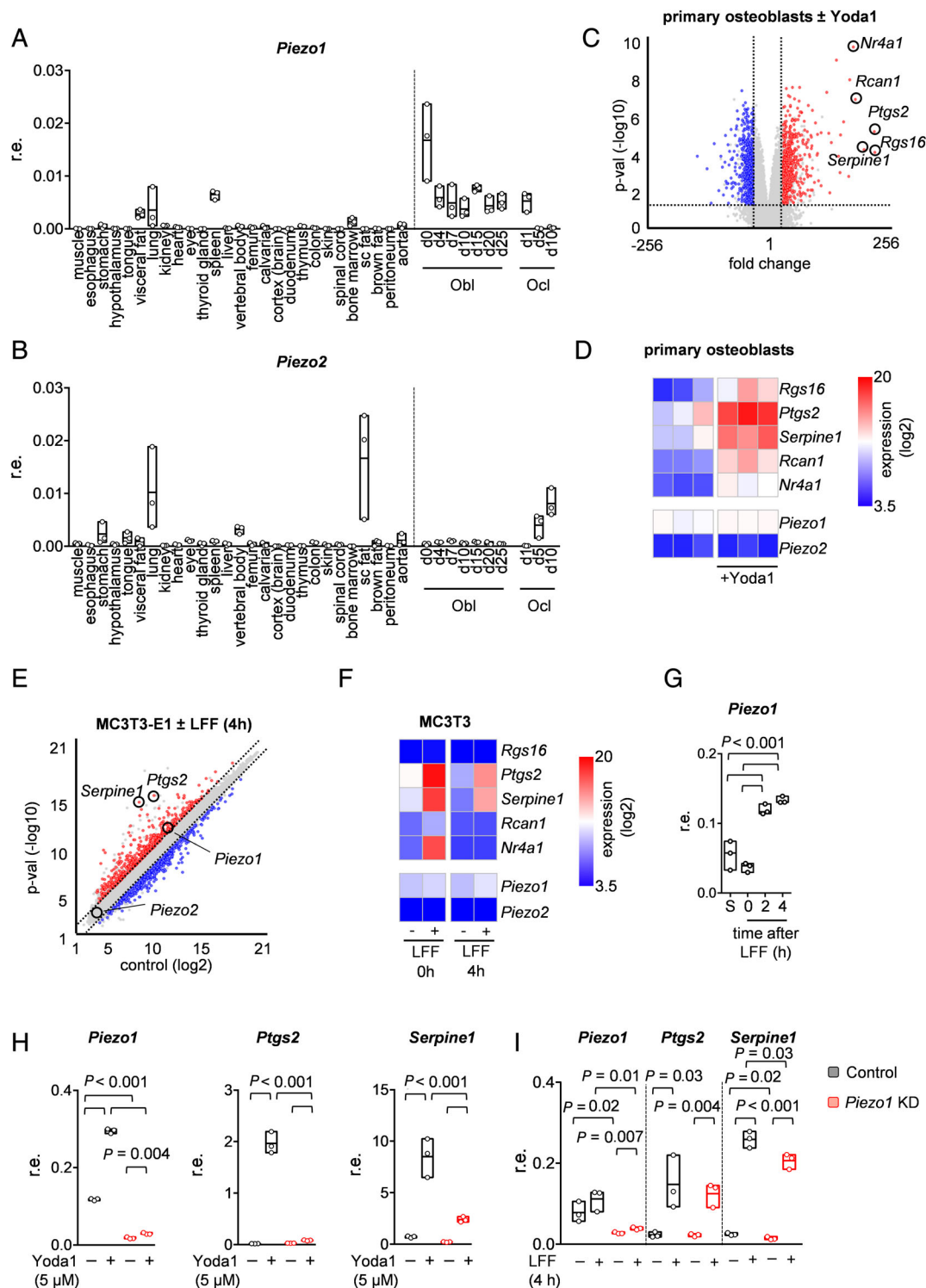


Fig 1. Piezo1 activation in osteoblasts induces the expression of mechanoresponsive genes. (A) qRT-PCR expression analysis of *Piezo1* and (B) *Piezo2* in different murine tissues and in primary bone cells at different stages of ex vivo differentiation. (C) Volcano plot showing differentially expressed genes in wild-type primary osteoblasts treated with the Piezo1 agonist Yoda1 (5 μ M) or DMSO for 6 hours. (D) Heat map showing the five genes with the strongest induction after Yoda1 administration, as well as *Piezo1* and *Piezo2*. Data are shown as log₂ expression values. (E) Scatter plots of single whole-transcriptome analyses of MC3T3-E1 cells 4 hours after mechanical stimulation by LFF. (F) Heat map illustrating the expression of a selection of genes in MC3T3-E1 cells 0 and 4 hours after mechanical stimulation by LFF. Data are shown as log₂ expression values. (G) qRT-PCR analysis of *Piezo1* expression in MC3T3-E1 cells under static (S) conditions and 0, 2, and 4 hours post-LFF. (H) qRT-PCR analysis of *Piezo1*, *Ptgs2*, and *Serpine1* in MC3T3-E1 cells treated with Yoda1 (5 μ M) and after siRNA-mediated KD of *Piezo1*. (I) qRT-PCR analysis of *Piezo1*, *Ptgs2*, and *Serpine1* in MC3T3-E1 cells 4 hours after mechanical stimulation by LFF and after siRNA-mediated knockdown of *Piezo1*. Data are median, minimum to maximum ($n = 3$), p values obtained by unpaired two-tailed t -test. KD = knockdown; LFF = laminar fluid flow; Obl = osteoblasts; Ocl = osteoclasts; S = static.

was unaffected by *Piezo1* knockdown 0 and 4 hours after exposure to LFF (Fig. 1I; Supplementary Fig. 1D). This unexpected discrepancy led us to generate mouse models with *Piezo1* and/or *Piezo2* inactivation in specific skeletal cell populations.

Runx2Cre-mediated *Piezo1* deletion causes a more severe osteoporotic phenotype than *Dmp1Cre*-mediated *Piezo1* deletion

We first took advantage of *Dmp1Cre* mice to inactivate the two Piezo proteins in terminally differentiated osteoblasts, that is osteocytes.⁽³⁸⁾ By undecalcified histology of the lumbar vertebral bodies and μ CT analysis of the femoral bones, we observed that *Piezo1^{Dmp1Cre}* mice displayed reduced trabecular and cortical bone mass, a phenotype that was not exacerbated by the combined deletion of both *Piezo* genes (Supplementary Fig. 2). The deduced hypothesis that only *Piezo1* is required for osteocyte mechanosensation was subsequently confirmed by an in vivo ulna loading experiment (Supplementary Fig. 3). Although these data are consistent with a recent study, where *Piezo1^{Dmp1Cre}* mice were subjected to tibia loading,⁽³⁴⁾ it was additionally important to analyze the cellular consequences of *Piezo1* deletion in osteocytes. In fact, whereas we did not detect significant changes in osteocyte number or the number of canalicular extensions after acid-etching of *Piezo1^{fl}* and *Piezo1^{Dmp1Cre}* cortical bone (Supplementary Fig. 4A,B), the osteoblast population was obviously affected. More specifically, we observed that trabecular osteoblasts in *Piezo1^{Dmp1Cre}* mice did not generally exhibit the characteristic cuboidal shape, but showed a flattened appearance (Supplementary Fig. 4C). Together with the initially observed high expression of *Piezo1* in osteoblast progenitor cells, these data suggested that *Piezo1* might have an additional function in osteoblast differentiation, independent of its role in osteocyte mechanosensation.

To delete *Piezo1* and/or *Piezo2* in osteoblast progenitor cells we took advantage of *Runx2Cre* mice, where recombination, unlike in *Prx1Cre* mice, occurs in all skeletal elements.⁽³⁹⁾ Moreover, because *Piezo2* was found to be expressed in differentiated osteoclasts, we additionally inactivated the two Piezo proteins in osteoclast lineage cells using *Lyz2Cre* mice.⁽⁴⁰⁾ We generated *Piezo1^{Runx2Cre}*, *Piezo1^{Lyz2Cre}*, *Piezo2^{Runx2Cre}*, and *Piezo2^{Lyz2Cre}* mice and analyzed their skeletal phenotypes in comparison to their respective Cre-negative littermates at 12 weeks of age. By undecalcified histology of vertebral bodies we identified a remarkable reduction of trabecular bone mass specifically in the *Piezo1-Runx2Cre* mice of both sexes (Fig. 2A,B). In comparison to *Piezo1-Dmp1Cre* mice, this phenotype was not only more severe, but also different, as it was strongly pronounced in the trabecular bone compartment below the growth plates (Supplementary Fig. 5). Whereas *Piezo1^{Lyz2Cre}* and *Piezo2^{Lyz2Cre}* mice did not display a detectable skeletal phenotype, a moderate reduction of trabecular bone mass was also identified in female, but not in male *Piezo2^{Runx2Cre}* mice. These trabecular bone phenotypes were confirmed by μ CT analysis of the femurs, where we additionally detected reduced cortical thickness and increased cortical porosity in *Piezo1^{Runx2Cre}* mice (Fig. 2C–E). *Piezo1^{Runx2Cre}* femurs were also significantly shorter in comparison to *Piezo1^{fl}* controls (Fig. 2F).

The most striking aspect of the *Piezo1^{Runx2Cre}* phenotype was, however, the high number of spontaneous fractures (Fig. 3A). More specifically, in 12-week-old *Piezo1^{Runx2Cre}* mice, we identified an average of five rib fractures and one hindlimb fracture per animal (Fig. 3B). In contrast, we rarely and never detected

fractures in *Piezo1^{Dmp1Cre}* and *Piezo2^{Runx2Cre}* mice, respectively. As an additional pathology in *Piezo1^{Runx2Cre}* mice we identified dysplasia of the pelvic bone on X-ray images, which was supported by μ CT analysis, where we observed an increased pelvic porosity and angle (Fig. 3C–E). Interestingly, a similar pathology was previously reported for mice subjected to microgravity for 1 month.⁽⁴⁹⁾ Finally, it is noteworthy that we did not detect an alteration of calvarial thickness or porosity in 12-week-old *Piezo1-Runx2Cre* mice (Fig. 3F,G), suggesting that deletion of *Piezo1* during early stages of osteoblast differentiation specifically affects bones that are formed through endochondral ossification.

Because we detected a moderate trabecular bone mass reduction in female *Piezo2^{Runx2Cre}* mice, we additionally analyzed *Piezo1;Piezo2^{Runx2Cre}* mice to investigate if the combined loss of both Piezo proteins would exacerbate the *Piezo1^{Runx2Cre}* phenotype. Because *Piezo1;Piezo2^{Runx2Cre}* mice were not viable until the age of 12 weeks, we analyzed them at a younger age. Here we identified a high incidence of fractures at 3 and 6 weeks of age (Supplementary Fig. 6A–C). In 6-week-old *Piezo1;Piezo2-Runx2Cre* mice we additionally identified reduced skeletal growth, near absence of trabecular bone, but no difference toward *Piezo1;Piezo2^{fl}* littermates in terms of growth plate morphology (Supplementary Fig. 6D–H). This unexpected early-onset phenotype did not only demonstrate that *Piezo2* can compensate, to some extent, for the loss of *Piezo1*, but also suggested a critical role for *Piezo1* in bone development by endochondral ossification.

Piezo1 controls the expression of chondrogenic genes

To understand the molecular basis of the bone phenotype of *Piezo1^{Runx2Cre}* mice, we analyzed the ex vivo behavior of *Piezo1-Runx2Cre* osteoblast progenitor cells. In bone marrow cultures we observed, by Alizarin red staining of mineralized matrix, 10 days after addition of ascorbic acid and β -glycerolphosphate, a significant ($p = .018$) reduction by 40% in *Piezo1^{Runx2Cre}* cultures. Because we also observed a cell-autonomous osteogenesis defect in primary calvarial osteoblasts isolated from *Piezo1-Runx2Cre* mice (Fig. 4A), we focused on their further analyses for two major reasons. First, there are far fewer other cell types in calvaria-derived cultures, which enhanced the possibility to uncover differentially expressed genes in independently isolated cultures. Second, incomplete closure of cranial sutures had been described for newborn *Piezo1^{OcnCre}* mice,⁽³³⁾ thereby suggesting an impact of *Piezo1* deficiency on craniofacial bone development. We therefore performed whole-transcriptome analyses with three independent *Piezo1^{fl}* and *Piezo1^{Runx2Cre}* primary calvarial osteoblast cultures at day 2 of differentiation. We thereby identified 15 genes with significant differential expression, one of them *Piezo1*, displaying the expected reduction in *Piezo1-Runx2Cre* osteoblasts (Fig. 4B). Unexpectedly, we detected increased expression of *Sox9* and *Cdkn1c*, both required, in mice and humans, for the coordinated differentiation of growth plate chondrocytes during endochondral bone formation.^(50,51) Moreover, we observed increased expression of *Deptor*, encoding an inhibitor of the mammalian target of rapamycin complex 1 and 2 (mTORC1, mTORC2) that induces autophagy and influences hypertrophic chondrocyte differentiation.^(52,53) The respective transcriptome changes were confirmed by qRT-PCR, and here we additionally detected increased expression of other chondrocyte differentiation markers, that is *Acan* and *Col10a1* (Fig. 4C). In contrast, *Vegfa*, encoding an angiogenic protein essential for

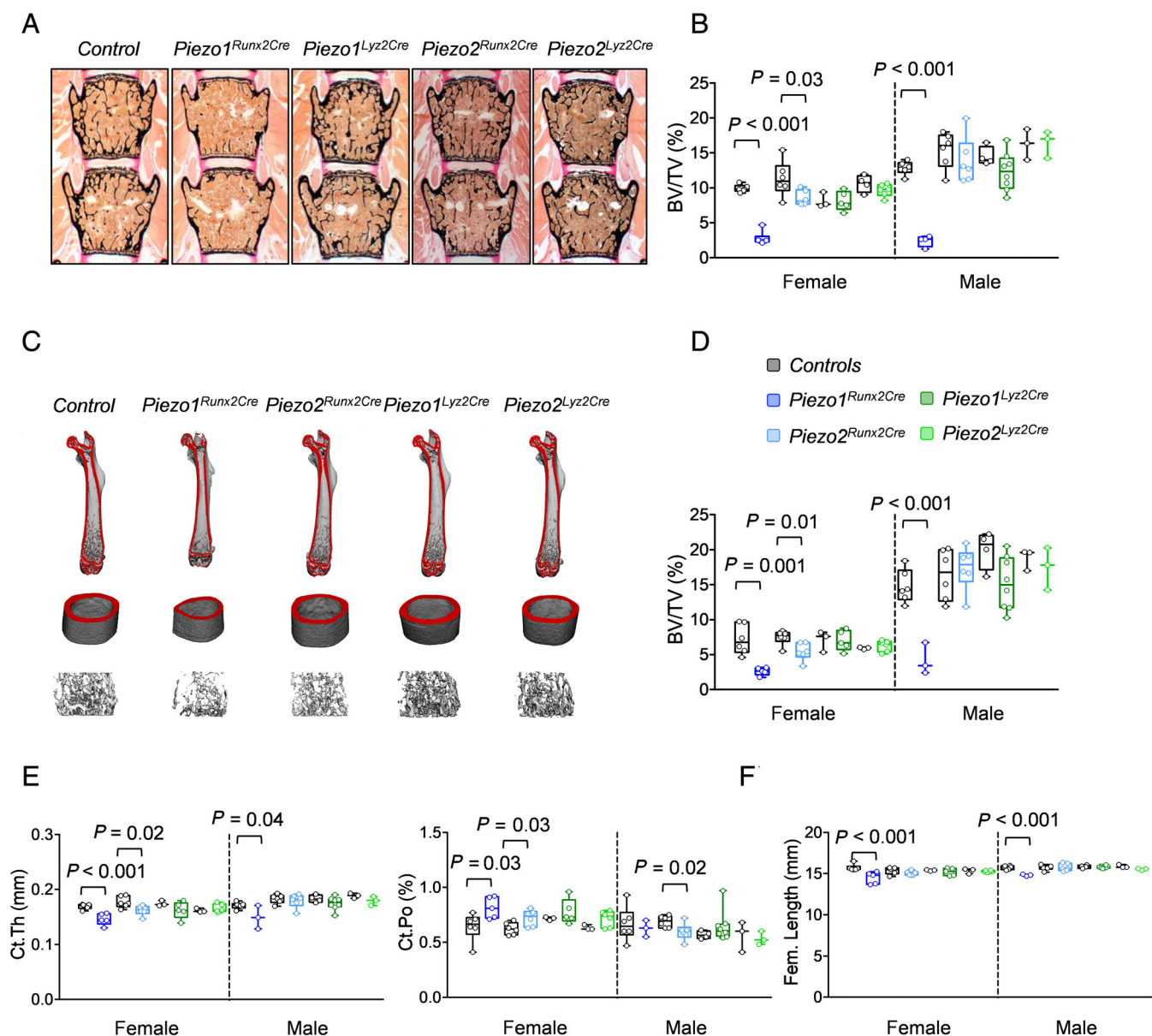


Fig 2. *Runx2Cre*-mediated *Piezo1* deletion causes a low bone mass phenotype. (A) Representative images after von Kossa staining of lumbar spine sections of 12-week-old female control, *Piezo1*^{Runx2Cre}, *Piezo1*^{Lyz2Cre}, *Piezo2*^{Runx2Cre}, and *Piezo2*^{Lyz2Cre} mice. (B) Quantification of the trabecular BV/TV in lumbar spine sections of 12-week-old female and male mice *Piezo1*^{Runx2Cre} ($n = 6$ female; $n = 4$ male), *Piezo2*^{Runx2Cre} ($n = 6$ female; $n = 6$ male), *Piezo1*^{Lyz2Cre} ($n = 6$ female; $n = 8$ male), and *Piezo2*^{Lyz2Cre} mice ($n = 6$ female; $n = 3$ male), in comparison to their respective *Cre*-negative *Piezo1*^{fl} or *Piezo2*^{fl} littermate controls. (C) Representative μ CT images showing whole femurs (top), cortical (middle), and trabecular bone (bottom) from 12-week-old female control, *Piezo1*^{Runx2Cre}, *Piezo2*^{Runx2Cre}, *Piezo1*^{Lyz2Cre}, and *Piezo2*^{Lyz2Cre} mice. (D) μ CT-based quantification of the trabecular BV/TV in 12-week-old female and male *Piezo1*^{Runx2Cre} ($n = 6$ female; $n = 4$ male), *Piezo2*^{Runx2Cre} ($n = 6$ female; $n = 6$ male), *Piezo1*^{Lyz2Cre} ($n = 6$ female; $n = 8$ male), and *Piezo2*^{Lyz2Cre} mice ($n = 6$ female; $n = 3$ male), in comparison to their respective *Cre*-negative *Piezo1*^{fl} or *Piezo2*^{fl} littermate controls. (E,F) μ CT-based quantification of Ct.Th, Ct.Po (E), and femur length (F) in the same mice. Data are median with interquartile range, whiskers indicate minimum to maximum, p values obtained by unpaired two-tailed t test. BV/TV = bone volume per tissue volume; Ct.Po = cortical porosity; Ct.Th = cortical thickness.

endochondral bone formation,⁽⁵⁴⁾ was transcriptionally downregulated in *Piezo1*^{Runx2Cre} osteoblasts.

As an established in vitro model of endochondral ossification,⁽⁵⁵⁾ we next cultured ATDC5 chondrogenic cells with or without Yoda1 starting on day 7 of differentiation, when chondrogenic media were changed to osteogenic media (Fig. 4D). After 3 days of Yoda1 treatment, ie, at day 10 of differentiation,

we did not only observe significantly increased *Piezo1* expression, but also a strong reduction in the expression of *Col10a1* (Fig. 4E). Although *Sox9*, *Acan*, and *Col2a1* remained transcriptionally unchanged, Yoda1 treatment also caused a reduction in *Deprt* and *Cdkn1c* expression, as well as a transcriptional activation of *Vegfa* (Fig. 4F). Of note, *Vegf* induction was also observed in primary osteoblasts after administration of Yoda1,

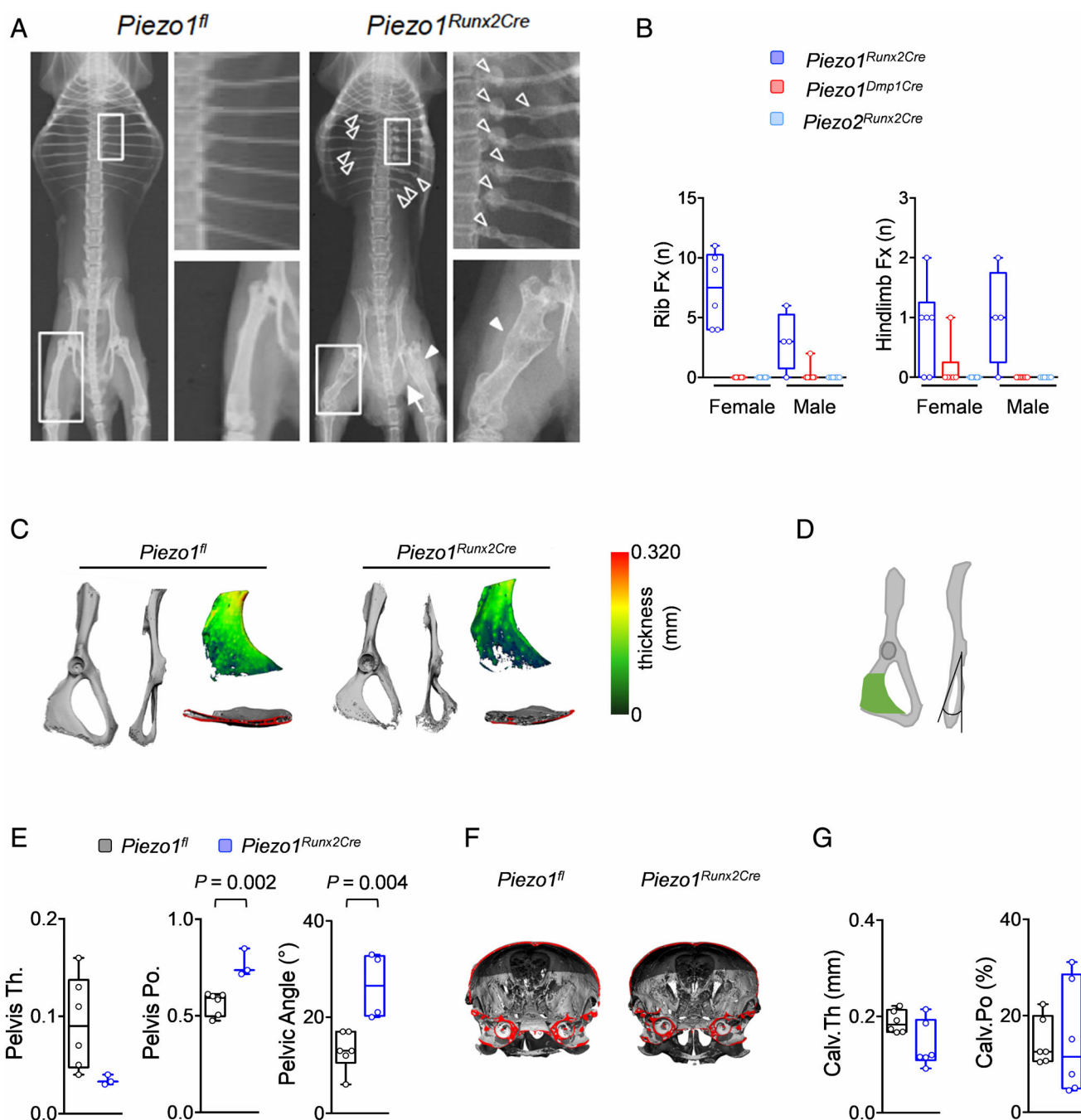


Fig 3. *Runx2Cre*-mediated *Piezo1* deletion causes spontaneous fractures and pelvic dysplasia. (A) Representative X-ray images of 12-week-old female *Piezo1^{fl}* and *Piezo1^{Runx2Cre}* mice. White boxes indicate magnified areas, showing multiple rib fractures (empty arrowheads), femoral fractures (closed arrowheads), and pelvic dysplasia (arrow). (B) Quantification of rib and hindlimb fractures in 12-week-old female and male *Piezo1^{Runx2Cre}* ($n = 6$ female, $n = 4$ male), *Piezo1^{Dmp1Cre}* ($n = 6$ female, $n = 7$ male), and *Piezo2^{Runx2Cre}* mice ($n = 6$ female, $n = 6$ male). (C) Representative μ CT images of pelvis and ischium from 12-week-old female *Piezo1^{fl}* and *Piezo1^{Runx2Cre}* mice. (D) Schematic representation of the pelvic bone, the ischium (green) and the pelvic angle. (E) Quantification of Pelvis Th., Pelvis Po., and pelvic angle in 12-week-old female *Piezo1^{fl}* ($n = 6$) and *Piezo1^{Runx2Cre}* mice ($n = 4$). (F) Representative μ CT images of the skull from 12-week-old female *Piezo1^{fl}* and *Piezo1^{Runx2Cre}* mice. (G) μ CT-based quantification of Calv.Th and Calv.Po in 12-week-old female *Piezo1^{fl}* ($n = 6$) and *Piezo1^{Runx2Cre}* mice ($n = 6$). Data are median with interquartile range, whiskers indicate minimum to maximum, p values obtained by unpaired two-tailed t test. Calv.Po = calvarial porosity; Calv.Th = calvarial thickness; Pelvis Po. = pelvic porosity; Pelvis Th. = pelvic thickness.

where Gene Ontology (GO) analysis of differentially expressed genes identified a significant enrichment for genes involved in VEGF signaling (Supplementary Fig. 7). We next addressed the question if siRNA-mediated knockdown of *Piezo1* in ATDC5 cells

would also affect the expression of chondrogenic markers. We therefore transfected the cells at day 7 of differentiation and monitored gene expression 2 and 3 days thereafter. Although the *Piezo1* knockdown was less pronounced compared to

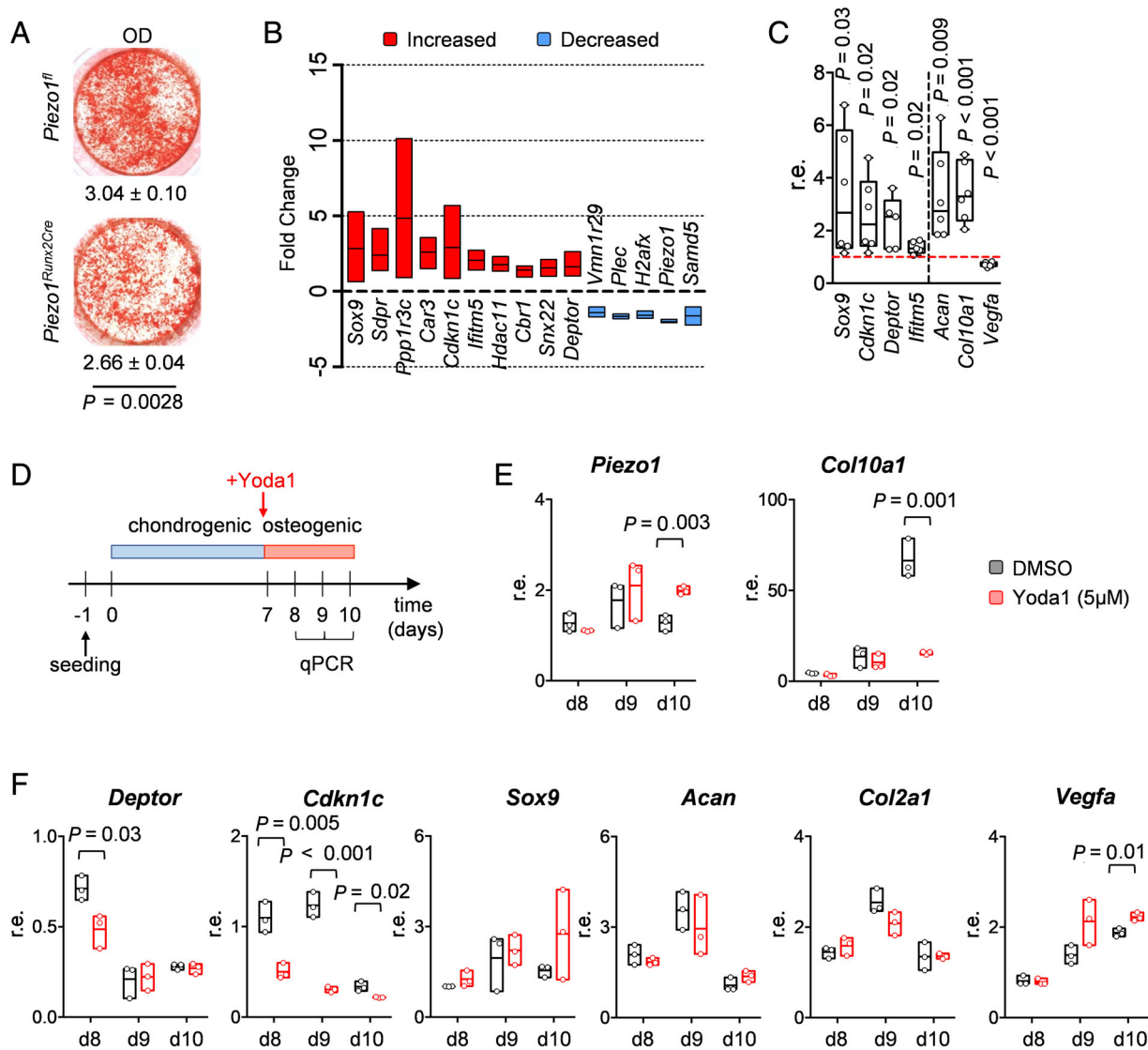


Fig 4. Piezo1 controls the expression of chondrogenic genes. (A) Alizarin red staining and OD quantification of matrix mineralization in primary calvarial osteoblast cultures from *Piezo1^{fl}* and *Piezo1^{Runx2Cre}* mice at day 10 of differentiation. (B) Graphic representation of all genes displaying significantly increased or decreased expression in *Piezo1^{Runx2Cre}* primary calvarial osteoblasts after whole-transcriptome analyses from three independent experiments. (C) Relative qRT-PCR expression analysis for the indicated genes in *Piezo1^{Runx2Cre}* primary osteoblasts. The red dotted line indicates the expression in *Piezo1^{fl}* control cultures. (D) Setup of the in vitro endochondral ossification assay with differentiating ATDC5 cells treated with or without Yoda1 (5µM). (E) qRT-PCR expression analysis of *Piezo1* and *Col10a1* in chondrogenic ATDC5 cells at day 8, 9, and 10 of differentiation, after treatment with vehicle (DMSO) or Yoda1. (F) qRT-PCR expression analysis of *Deftor*, *Cdkn1c*, *Sox9*, *Acan*, *Col2a1*, and *Vegf* in the same samples. Data are either median with interquartile range, whiskers indicate minimum to maximum or median and minimum to maximum, p values obtained by unpaired two-tailed t test. OD = optical density.

MC3T3-E1 cells, we observed a moderate induction of *Col10a1*, *Acan*, and *Col2a1* (Supplementary Fig. 8A). To confirm these data through an independent experimental approach, we added GsMTx4 (4µM), a spider venom peptide that is commonly used to inhibit Piezo1,⁽³³⁾ to the culture medium. This treatment did not only increase the expression of the above-mentioned chondrogenic markers, but also of *Deftor* and *Sox9* (Supplementary Fig. 8B). Taken together, these fully unexpected data, based on an unbiased analysis of primary calvarial osteoblasts, led us to focus on the role of Piezo1 in endochondral ossification and to analyze, as a next step, *Piezo1^{Runx2Cre}* mice at younger age.

Runx2Cre-mediated Piezo1 deletion impairs secondary spongiosa formation

To identify the age of onset of the *Piezo1^{Runx2Cre}* phenotype, we first analyzed newborn *Piezo1^{fl}* and *Piezo1^{Runx2Cre}* littermates. Here we did not detect obvious skeletal defects or fractures immediately after birth (Fig. 5A). Moreover, newborn *Piezo1^{Runx2Cre}* did not display the calvarial bone defect previously described for *Piezo1^{OcnCre}* mice (Fig. 5B), and their trabecular bone mass was not decreased compared to *Piezo1^{fl}* littermates in vertebral body sections (Fig. 5C). However,

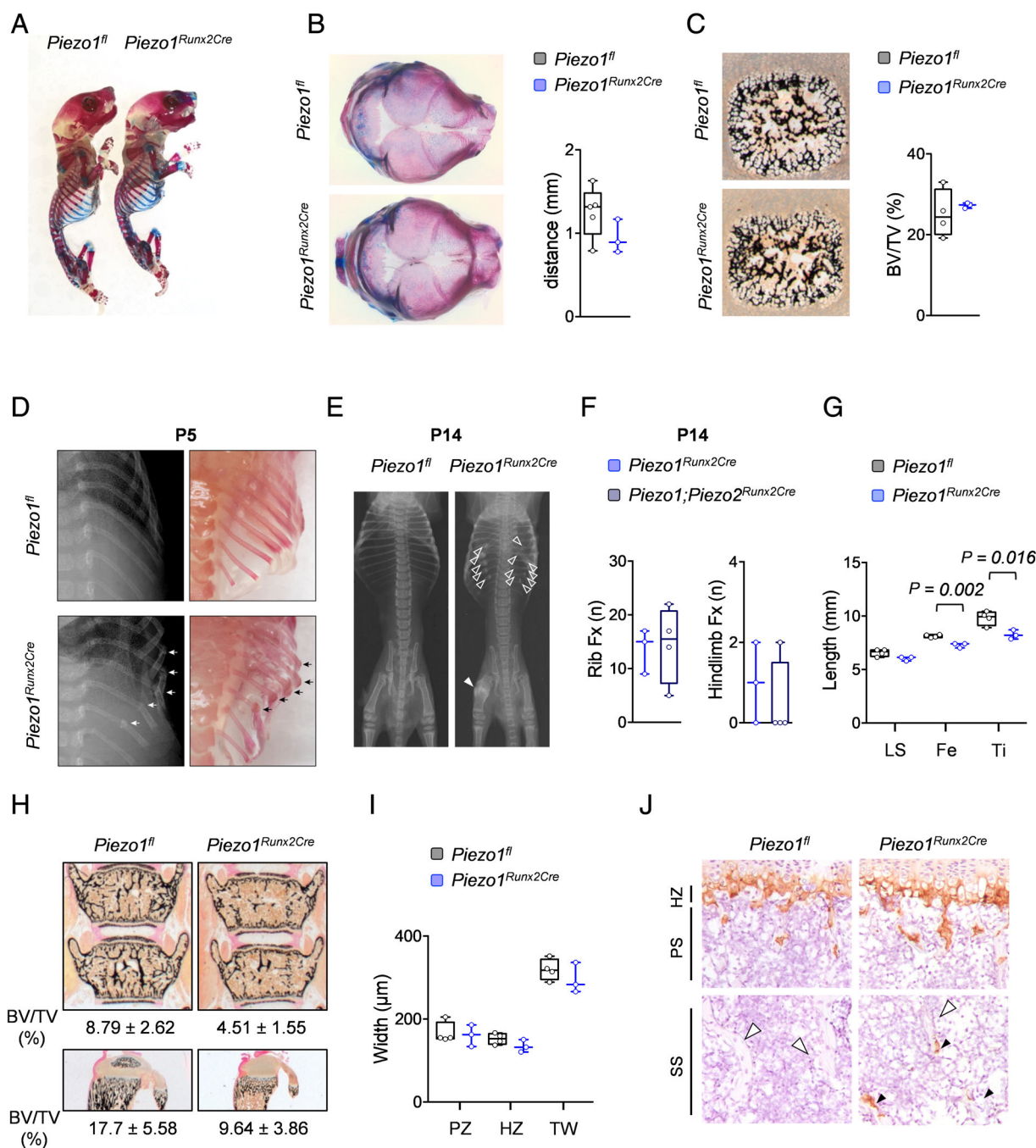


Fig 5. The *Piezo1^{Runx2Cre}* skeletal phenotype develops in an early postnatal phase. (A) Representative images of Alizarin red/Alcian blue staining from *Piezo1^{fl}* and *Piezo1^{Runx2Cre}* full skeletons at birth (P0). (B) Representative Alizarin red/Alcian blue staining from *Piezo1^{fl}* and *Piezo1^{Runx2Cre}* calvaria and quantification of distance between parietal bones at birth (P0). (C) Representative von Kossa staining and quantification of trabecular BV/TV of lumbar spine sections from 1-day-old female *Piezo1^{fl}* ($n = 4$) and *Piezo1^{Runx2Cre}* mice ($n = 3$). (D) Representative images of X-rays and Alizarin red/Alcian blue staining of *Piezo1^{fl}* and *Piezo1^{Runx2Cre}* at P5 showing multiple rib fractures (arrows). (E) Representative X-ray images of female 2-week-old *Piezo1^{fl}* and *Piezo1^{Runx2Cre}* mice showing multiple rib fractures (empty arrowheads) and a femoral fracture (full arrowhead). (F) Quantification of rib and hindlimb fractures in 2-week-old female *Piezo1^{Runx2Cre}* ($n = 3$) and *Piezo1;Piezo2^{Runx2Cre}* mice ($n = 4$). (G) X-ray-based quantification of length of LS, Fe, and Ti in 2-week-old female *Piezo1^{fl}* ($n = 4$) and *Piezo1^{Runx2Cre}* mice ($n = 3$). (H) Representative von Kossa staining and quantification of trabecular BV/TV of lumbar spine (top) and tibia sections (bottom) from 2-week-old female *Piezo1^{fl}* ($n = 4$) and *Piezo1^{Runx2Cre}* mice ($n = 3$). (I) Quantification of the PZ, HZ, and TW in 2-week-old female *Piezo1^{fl}* ($n = 4$) and *Piezo1^{Runx2Cre}* mice ($n = 3$). (J) Immunohistochemistry staining for collagen type X showing ColX-positive (full arrowheads) and ColX-negative (empty arrowheads) trabecular bone cells in LS sections of 2-week-old male *Piezo1^{fl}* and *Piezo1^{Runx2Cre}* mice. The localization of the HZ as well as the PS and SS is indicated on the left. Data are median with interquartile range, whiskers indicate minimum to maximum, p values obtained by unpaired two-tailed t test. BV/TV = bone volume per tissue volume; Fe = femurs; HZ = hypertrophic zone; LS = lumbar spine; P0 = postnatal day 0; PS = primary spongiosa; PZ = proliferative zone; SS = secondary spongiosa; Ti = tibias; TW = total growth plate width.

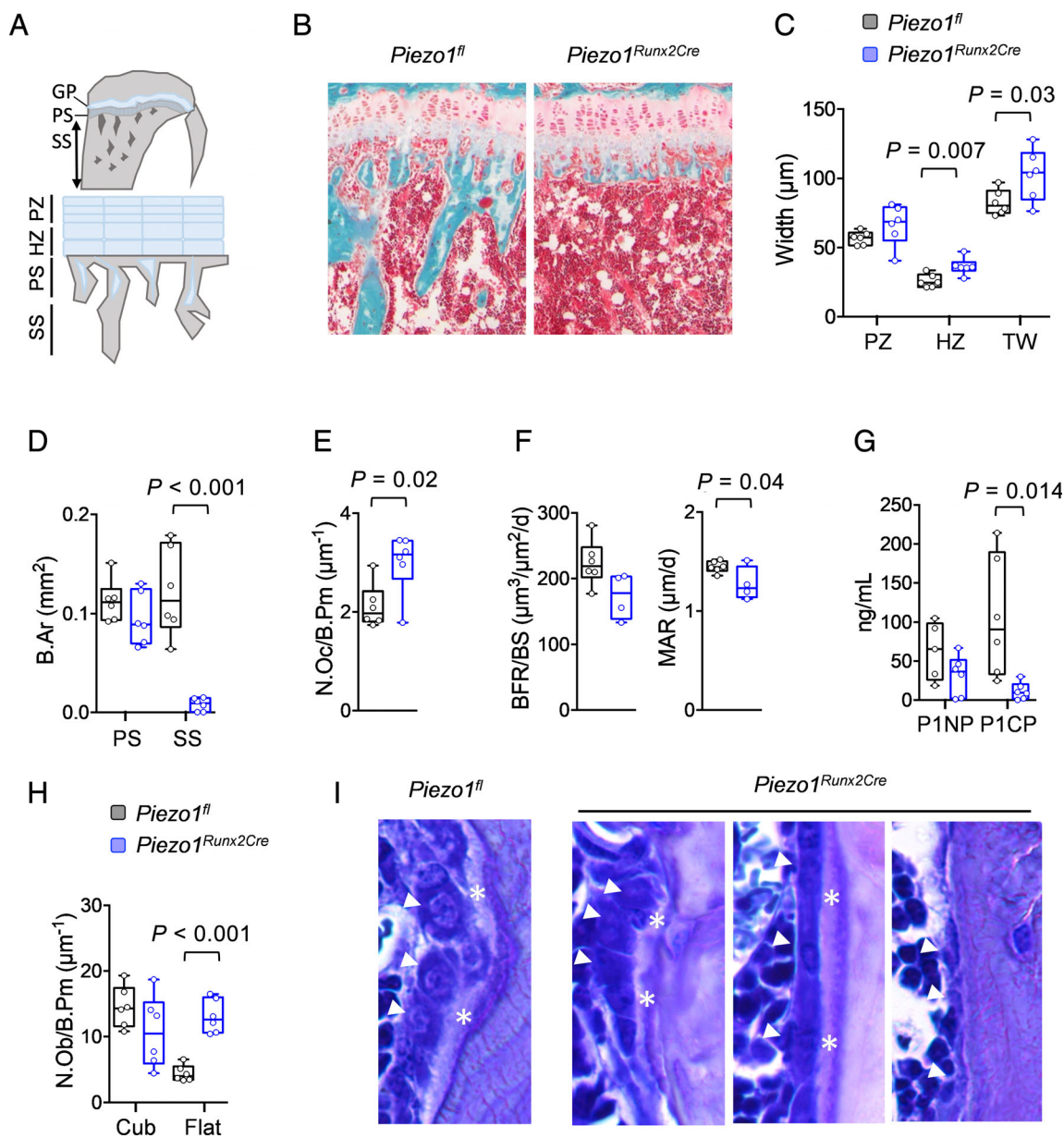


Fig 6. *Runx2Cre*-mediated *Piezo1* deletion impairs endochondral ossification and secondary spongiosa formation. (A) Schematic representation of the GP with PZ and HZ as well as the areas comprising the PS and SS. (B) Representative tibia sections of 12-week-old female *Piezo1*^{fl/fl} and *Piezo1*^{Runx2Cre} mice after Masson-Goldner trichrome staining. (C) Quantification of the PZ, HZ, and TW in 12-week-old female *Piezo1*^{fl/fl} (*n* = 6) and *Piezo1*^{Runx2Cre} mice (*n* = 6). (D) Quantification of the B.Ar comprising the PS and SS in the same animals. (E) Number of osteoclasts (N.Oc/B.Pm) on trabecular bone surfaces in lumbar spine sections of 12-week-old female *Piezo1*^{fl/fl} (*n* = 6) and *Piezo1*^{Runx2Cre} mice (*n* = 6). (F) Dynamic histomorphometric analysis of the trabecular BFR/BS and MAR in the same animals. (G) Serum P1NP and P1CP concentrations in 12-week-old female *Piezo1*^{fl/fl} (*n* = 5) and *Piezo1*^{Runx2Cre} mice (*n* = 6). (H) Quantification of the number of cuboidal and flattened osteoblasts (N.Ob/B.Pm) in 12-week-old female *Piezo1*^{fl/fl} (*n* = 6) and *Piezo1*^{Runx2Cre} mice (*n* = 6). (I) Representative toluidine blue staining of trabecular bone surfaces in lumbar spine sections showing cuboidal osteoblasts (arrowheads) with osteoid (asterisks) in 12-week-old female *Piezo1*^{fl/fl} mice, as well as cuboidal (left, arrowheads) or flattened osteoblasts (middle, arrowheads) with osteoid (asterisks) and bone lining cells (right) in 12-week-old female *Piezo1*^{Runx2Cre} mice. Data are median with interquartile range, whiskers indicate minimum to maximum, *p* values obtained by unpaired two-tailed *t* test. B.Ar = bone area; BFR/BS = bone formation rate per bone surface; GP = growth plate; HZ = hypertrophic zone; MAR = mineral apposition rate; N.Oc/B.Pm = number of osteoclasts/bone perimeter; PS = primary spongiosa; PZ = proliferative zone; SS = secondary spongiosa; TW = total growth plate width.

already at postnatal day 5 (P5) the first rib fractures appeared (Fig. 5D), and at 2 weeks of age all *Piezo1*^{Runx2Cre} mice displayed skeletal fractures (Fig. 5E). Importantly, the number of fractures at that age was comparable to *Piezo1*;*Piezo2*^{Runx2Cre}

mice (Fig. 5F), thereby confirming that *Piezo1* is the most relevant *Piezo* channel to achieve skeletal integrity. In 2-week-old *Piezo1*^{Runx2Cre} mice, we additionally detected shortening of the long bones (Fig. 5G), suggesting impaired endochondral

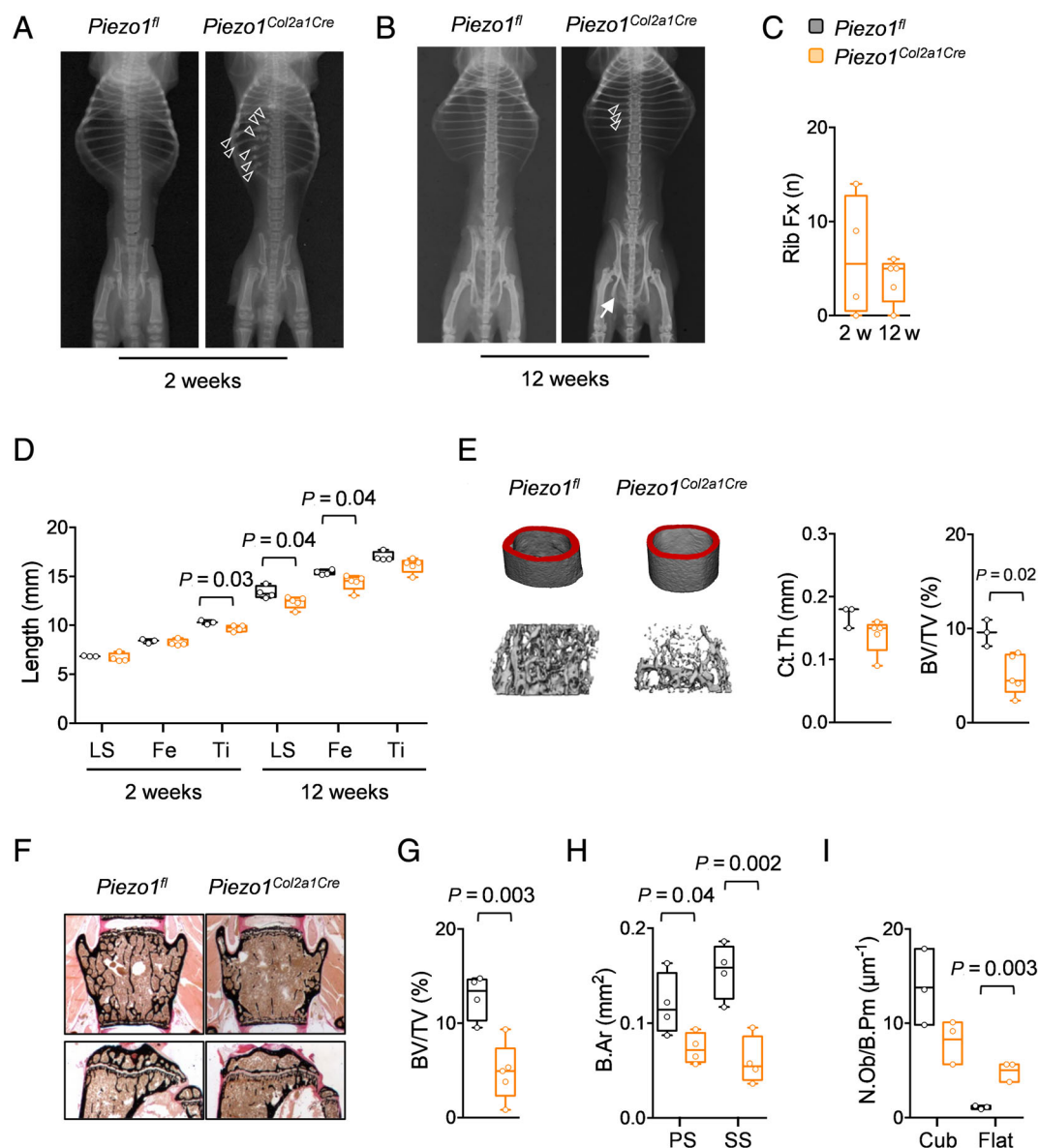


Fig 7. *Col2a1Cre*-mediated *Piezo1* deletion impairs trabecular bone formation. (A) Representative X-ray images of 2-week-old female *Piezo1^{fl}* and *Piezo1^{Col2a1Cre}* mice demonstrating multiple rib fractures (empty arrowheads). (B) X-ray images of 12-week-old female *Piezo1^{fl}* and *Piezo1^{Col2a1Cre}* mice demonstrating rib fractures (empty arrowheads) and pelvic dysplasia (arrow). (C) Quantification of rib fractures in female *Piezo1^{Col2a1Cre}* mice at 2 weeks (2w, $n = 4$) and 12 weeks (12w, $n = 5$) of age. (D) X-ray-based quantification of the length of LS, Fe, and Ti in 2-week-old and 12-week-old female *Piezo1^{fl}* and *Piezo1^{Col2a1Cre}* mice. (E) Representative μ CT images of cortical (top) and trabecular bone (bottom) from femora of 12-week-old female *Piezo1^{fl}* ($n = 4$) and *Piezo1^{Col2a1Cre}* mice ($n = 5$). Quantification of Ct.Th and trabecular BV/TV is given on the right. (F) Von Kossa staining of lumbar spine (top) and tibia sections (bottom) from 12-week-old female *Piezo1^{fl}* and *Piezo1^{Col2a1Cre}* mice. (G) Quantification of trabecular BV/TV in the LS of 12-week-old female *Piezo1^{fl}* ($n = 4$) and *Piezo1^{Col2a1Cre}* mice ($n = 5$). (H) Analysis of the B.Ar comprising the PS and SS in 12-week-old female *Piezo1^{fl}* ($n = 4$) and *Piezo1^{Col2a1Cre}* mice ($n = 5$). (I) Quantification of the number of cuboidal and flattened osteoblasts (N.Ob/B.Pm) on trabecular bone surfaces in the LS of the same mice. Data are either median with interquartile range, whiskers indicate minimum to maximum or median and minimum to maximum, p values obtained by unpaired two-tailed t test. B.Ar = bone area; BV/TV = bone volume per tissue volume; Ct.Th = cortical thickness; Fe = femurs; LS = lumbar spine; N.Ob/B.Pm = number of osteoblasts/bone perimeter; PS = primary spongiosa; SS = secondary spongiosa; Ti = tibias.

ossification. Importantly however, whereas the trabecular bone volume was reduced in these mice (Fig. 5H), their growth plate morphology was unaffected (Fig. 5I). This was also confirmed by immunohistochemistry for type X collagen, where we additionally made an unexpected observation. More

specifically, whereas type X collagen was only detected in hypertrophic cartilage and the primary spongiosa in *Piezo1^{fl}* control mice, the presumptive osteoblasts of the secondary spongiosa in *Piezo1^{Runx2Cre}* mice were also positive for type X collagen (Fig. 5J).

Based on these findings we analyzed the growth plates in tibia sections from 12-week-old *Piezo1^{fl}* and *Piezo1^{Runx2Cre}* littermate mice (Fig. 6A,B). Here we identified an enlargement of the hypertrophic zones in *Piezo1^{Runx2Cre}* sections, although the difference toward *Piezo1^{fl}* controls was moderate (Fig. 6C). Most importantly, however, whereas the primary spongiosa was unaffected, the trabecular bone area comprising the secondary spongiosa was remarkably reduced in *Piezo1^{Runx2Cre}* mice (Fig. 6D), similar to what was found in the spine. Although there were only few trabecular structures present on *Piezo1^{Runx2Cre}* vertebral sections, we additionally used these to perform cellular and dynamic histomorphometry. Here we identified an increased osteoclast number (Fig. 6E) and a moderate reduction in the mineral apposition rate at the trabecular bone surfaces (Fig. 6F). Although these changes are in principal agreement with recently published findings in *Piezo1^{PrxCre}* mice,^(35,36) these histomorphometric data have to be regarded cautiously, given the strong reduction of trabecular number in *Piezo1^{Runx2Cre}* bone sections. The same applies for the serum concentrations of the bone formation biomarkers P1NP and P1CP, that is the amino-terminal and carboxy-terminal propeptides of type I collagen, that were found reduced in 12-week-old *Piezo1^{Runx2Cre}* mice compared to *Piezo1^{fl}* littermates (Fig. 6G).

What was most evident, however, was a changed morphology of *Piezo1^{Runx2Cre}* osteoblasts, similar to *Piezo1^{Dmp1Cre}* mice, but more pronounced. In fact, we detected a threefold increase in the number of osteoblasts with flattened appearance in 12-week-old *Piezo1^{Runx2Cre}* mice, when compared to *Piezo1^{fl}* controls (Fig. 6H). Here it is also important to state that we do not consider this pathology as an artifact of sectioning, especially because it was not observed in *Piezo2^{Runx2Cre}* mice or *Piezo1^{Lyz2Cre}* mice. Moreover, the unusually flattened osteoblasts in *Piezo1^{Runx2Cre}* mice were clearly distinguishable from bone lining cells, because they were placed over a layer of osteoid (Fig. 6I). Finally, the coexistence of cuboidal osteoblasts, flattened osteoblasts, and lining cells in individual vertebral body sections of *Piezo1^{Runx2Cre}* mice further illustrates that this is a unique aspect of their phenotype. Taken together, our collective findings show that *Piezo1^{Runx2Cre}* mice do not display a profound skeletal pathology at birth, but thereafter they develop a severe phenotype, which is primarily characterized by impaired formation of the secondary spongiosa.

Col2a1Cre-mediated Piezo1 deletion impairs trabecular bone formation

Because there is increasing evidence supporting the concept that trabecular bone osteoblasts derive from growth plate progenitor cells,^(56,57) the collective data obtained in *Piezo1^{Runx2Cre}* mice raised the hypothesis that the impact of Piezo1 on endochondral ossification is mediated by its influence on growth plate chondrocytes, where *Runx2* is also expressed.^(58,59) Therefore, to analyze the impact of Piezo1 inactivation in chondrocytes in vivo, we took advantage of *Col2a1Cre* mice⁽⁴¹⁾ to generate *Piezo1^{Col2a1Cre}* animals. Similar to *Piezo1^{Runx2Cre}* mice, there was a high incidence of skeletal fractures in *Piezo1^{Col2a1Cre}* mice, and 12-week-old animals also displayed pelvic dysplasia (Fig. 7A–C). We additionally observed a moderate reduction in the length of different skeletal elements in *Piezo1^{Col2a1Cre}* mice (Fig. 7D). By μ CT analysis of the femoral bones we observed that chondrocyte-specific Piezo1 inactivation did not significantly reduce cortical bone thickness, but that the trabecular bone

volume in *Piezo1^{Col2a1Cre}* mice was nearly 50% reduced compared to *Piezo1^{fl}* littermate controls (Fig. 7E).

That chondrocyte expression of *Piezo1* is required for trabecular bone formation was further confirmed by undecalcified histology of vertebral bodies and tibias (Fig. 7F). Here we detected a significantly reduced trabecular bone volume in *Piezo1^{Col2a1Cre}* mice, which was most pronounced in the secondary spongiosa (Fig. 7G,H). Finally, similar to *Piezo1^{Runx2Cre}* mice, the number of flattened osteoblasts was strongly increased in *Piezo1^{Col2a1Cre}* animals (Fig. 7I). On the other hand, osteoclast number and mineral apposition rate were not significantly different between 12-week-old *Piezo1^{fl}* and *Piezo1^{Col2a1Cre}* littermates (Supplementary Fig. 9), but also in this comparison, the results have to be regarded cautiously, because there were only a few trabeculae on *Piezo1^{Col2a1Cre}* bone sections. Despite this limitation, however, these data show that Piezo1 has a previously unrecognized function in chondrocytes to promote trabecular bone formation.

Discussion

Taken together, our findings, obtained through systematic analysis of mouse models with inactivation of Piezo1 and/or Piezo2 in different skeletal cell populations, revealed that Piezo1 has two independent functions in osteoblast lineage cells. First, thereby confirming data by others,⁽³⁴⁾ Piezo1 is required for mechanosensation by osteocytes. Second, Piezo1 expression in chondrocytes is required to generate the secondary spongiosa and thereby the trabecular bone compartment, a function that is relevant postnatally, underscored by the lack of a skeletal phenotype in newborn *Piezo1^{Runx2Cre}* mice. Therefore, our study provides a novel key information regarding the role of Piezo1 in the skeleton. In fact, based on the combined analyses from different investigators, which were all published very recently, it is now evident that mechanosensation through Piezo1 is critical for various aspects of skeletal development, growth, and remodeling.

It was initially reported that poking-induced mechanical responses of the osteoblast cell line MC3T3-E1 depend on *Piezo1* expression, and that *Piezo1^{OcnCre}* mice display a low bone mass phenotype due to decreased bone formation.⁽³³⁾ Because there was also a diminished response of *Piezo1^{OcnCre}* mice in the osteoanabolic response toward treadmill exercise, these data suggested that Piezo1 is the long-sought mechanoreceptor in the context of bone remodeling. That this critical function of Piezo1 depends on its expression in osteocytes was supported in a second study, which included the generation and analysis of *Piezo1^{Dmp1Cre}* mice.⁽³⁴⁾ Here the authors observed a low bone mass phenotype associated with spontaneous fracture in 16% of the animals. They additionally demonstrated that the osteoanabolic response of *Piezo1^{Dmp1Cre}* mice towards tibia loading is strongly reduced. Although our own data obtained in *Piezo1^{Dmp1Cre}* mice essentially confirm these previous findings, we included them as supplemental information, because it is important to show that the influence of loading in another skeletal element (ie, ulna) also depends on *Piezo1* expression in osteocytes. Moreover, it is further relevant to state that our analysis of the osteocyte lacunar network in *Piezo1^{Dmp1Cre}* mice, which has not been studied previously, revealed no major difference compared to *Piezo1^{fl}* controls, thereby showing that Piezo1 specifically controls mechanosensation without affecting osteocyte differentiation or morphology. Finally, by additionally generating *Piezo1[;] Piezo2^{Dmp1Cre}* mice, we are able to conclude that the potential

role of Piezo2 is neglectable in the context of osteocyte-regulated bone remodeling. This latter notion is also relevant with respect to our initial in vitro experiments using MC3T3-E1 cells. In fact, our observation that siRNA-mediated knockdown of Piezo1 did not abolish the LFF-induced *Ptgs2* expression is quite similar to what was found in the osteocyte cell line MLO-Y4.⁽³⁴⁾ This implies that Piezo-independent mechanisms have to exist, which participate in these LFF responses, at least in vitro.

That Piezo1 plays a critical role in the bone modeling phase, which became the primary focus of our manuscript, was also reported.^(35,36) It was shown that *Piezo1^{Prx1Cre}* mice, which substantially differ from the *Piezo1^{Runx2Cre}* mice, because Piezo1 inactivation does not take place in the axial skeleton, display an early-onset osteoporotic phenotype with a high incidence of spontaneous fractures. There are, however, remarkable differences in the phenotype pathogenesis between the two studies. In fact, whereas the first study identified excessive osteoclastogenesis as the major cause of the osteoporotic phenotype in 6-week-old *Piezo1^{Prx1Cre}* mice,⁽³⁵⁾ the second study identified a reduced bone formation rate in 3-week-old *Piezo1^{Prx1Cre}* mice as the major driver of the phenotype.⁽³⁶⁾ In this regard it is relevant to state that our histomorphometric analysis of *Piezo1^{Runx2Cre}* mice, although this has to be cautiously interpreted (due to a low amount of bone surfaces in the mutant animals), revealed a combination of both cellular phenotype causes. In fact, we identified a moderately increased osteoclast number together with reduced mineral apposition rate and serum P1CP concentration in 12-week-old *Piezo1^{Runx2Cre}* mice. These findings principally support the previously established function of Piezo1 in osteoblast–osteoclast coupling, molecularly explained by Piezo1-regulated production of Col2a1 and Col9a2 in osteoblasts, which in turn inhibit osteoclastogenesis.⁽³⁵⁾ Importantly, however, whereas the *Piezo1^{Prx1Cre}* mice used in the respective study were found to display a remarkable cortical bone porosity,⁽³⁵⁾ this parameter was only moderately increased in *Piezo1^{Runx2Cre}* animals. In any case, should there be a critical impact of Piezo1 on osteoclastogenesis, such an influence is likely mediated indirectly, because we confirmed that loss of Piezo1 in the osteoclast lineage (previously studied in *Piezo1-CstkCre* mice) does not cause a bone phenotype, and the same applies for Piezo2. With respect to *Prx1Cre* models it is finally relevant to state that a near absence of secondary spongiosa formation was noted in *Piezo1;Piezo2^{Prx1Cre}* mice, although this was not considered to be linked to *Piezo1* expression in chondrocytes.⁽³⁶⁾

Our focus on the potential role of Piezo1 in growth plate chondrocytes was triggered by the unexpected findings obtained by genomewide expression analysis of primary calvarial osteoblasts from *Piezo1^{fl}* and *Piezo1^{Runx2Cre}* mice, where we identified a remarkable increase in the expression of chondrogenic markers in the latter. In particular *Sox9*, encoding a key transcription factor promoting chondrogenic and inhibiting osteogenic differentiation,⁽⁵⁰⁾ was the most strongly induced gene in early-stage *Piezo1^{Runx2Cre}* osteoblasts. Because we also found an induction of *Col10a1* expression in *Piezo1^{Runx2Cre}* osteoblasts, together with a repression of *Col10a1* expression by Yoda1 administration to ATDC5 cells, we performed immunohistochemistry to detect type X collagen, an established marker for hypertrophic chondrocytes. Here we found, in tibia sections from *Piezo1^{Runx2Cre}* mice, unlike was the case in *Piezo1^{fl}* control sections, that the cells covering the surface of the nearly absent secondary spongiosa in *Piezo1^{Runx2Cre}* mice were positive for type X collagen. Because there is accumulating evidence that trabecular bone

osteoblasts, at least in the bone modeling phase, are derived from growth plate chondrocytes,^(56,57) these data suggested that the osteogenic differentiation of these progenitors is impaired in *Piezo1^{Runx2Cre}* mice. Our deduced hypothesis that Piezo1 is required to regulate the differentiation of growth plate osteochondroprogenitor cells was further investigated by the generation and analysis of *Piezo1^{Col2a1Cre}* mice. Here we identified, for the first time, that *Piezo1* inactivation in chondrocytes strongly affects secondary spongiosa formation due to impaired generation of trabecular osteoblasts, which results in a severe osteoporotic phenotype that is comparable to *Piezo1^{Runx2Cre}* mice. Since *Runx2* is not only expressed in osteoblast progenitors, but also in prehypertrophic chondrocytes,^(58,59) this phenotypic overlap between *Piezo1^{Col2a1Cre}* and *Piezo1^{Runx2Cre}* mice is concordant. Importantly however, future research toward the potential role of Piezo1 in the transdifferentiation of growth plate chondrocytes into trabecular osteoblasts, with for instance lineage tracing studies, is required to ultimately confirm our findings based on the phenotypes of *Piezo1^{Runx2Cre}* and *Piezo1^{Col2a1Cre}* mice.

It is also still required to understand the molecular mechanisms that explain how mechanosensation by Piezo1 is translated into a regulation of osteochondrogenic differentiation. However, because it may require complex cellular interactions controlled by specific mechanical forces that only exist in the in vivo setting, such an influence might be difficult to recapitulate in vitro. Therefore, although we truly believe in the value of cell culture systems to generate hypotheses, the respective results might not generally relate to the physiological situation. In our case it was for instance surprising that we identified increased expression of chondrogenic markers in *Piezo1^{Runx2Cre}* primary calvarial osteoblasts, although we retrospectively discovered that even newborn *Piezo1^{Runx2Cre}* mice do not display a calvarial bone phenotype. Similarly, although an altered osteoblast morphology was one of the most obvious pathologies observed in *Piezo1^{Runx2Cre}* bone sections, we did not detect an obvious impact of Piezo1 inactivation on morphology and cytoskeletal organization in cultured MC3T3-E1 cells or primary osteoblasts.

It is also noteworthy that our initial transcriptomic analyses did not pick up several previously established Piezo1 target genes.^(33–35) The strongest induction that we observed was related to *Cyr61*, which was more than sixfold induced in MC3T3-E1 cells 4 hours after LFF, similar to what has been reported for the osteocyte cell line MLO-Y4.⁽³⁴⁾ What we did not observe, however, unlike was reported for MLO-Y4 cells, was an induction of *Wnt1* expression by either LFF or Yoda1. Because *Wnt1* induction in osteocytes has been suggested to be essential for translating the Piezo1-mediated mechanical response into increased bone formation,⁽⁶⁰⁾ the absence of *Wnt1* induction in osteoblasts is a potentially relevant finding. In this regard it is further important to state that we have previously studied the skeletal phenotype of *Wnt1^{Runx2Cre}* mice, which displayed reduced bone mass and spontaneous fractures, but no impairment of secondary spongiosa formation.⁽⁶¹⁾ This essentially demonstrates that *Wnt1* is not a relevant downstream mediator of Piezo1 in the context of endochondral ossification, thereby further supporting our conclusion that Piezo1 has distinct functions in osteocytes and osteoprogenitor cells.

Although several questions regarding the role of Piezo1 in skeletal biology remain to be addressed, it is now evident, based on the combined data accumulated by different investigators, that Piezo1 is required for promoting bone formation in both, the modeling and remodeling phase. In this context it is highly

relevant that another recent study has confirmed that genetic variation in *PIEZO1* is associated with bone mineral density and fracture risk in humans.⁽⁶²⁾ Therefore, *PIEZO1* can be regarded as a potential osteoanabolic drug target for the treatment of skeletal disorders, including osteoporosis. Given the broad expression and the pleiotropic role of *PIEZO1* in various cell types, it is surely debatable, if selective *PIEZO1* activation would specifically enhance skeletal development or remodeling. However, because osteoporosis is most frequently observed in elderly patients, often associated with low physical activity, it is certainly worthwhile to optimize *PIEZO1*-specific agonism. Here it is important to state that treatment with the *Piezo1*-agonist *Yoda1* was previously shown to increase bone formation in wild-type mice, albeit only marginally.⁽³⁴⁾ Because this might be explained by suboptimal pharmacokinetic properties of *Yoda1*, the development of new *Piezo1* activators^(63,64) should certainly be intensified and assessed in vivo in the near future.

Disclosures

All authors state that they have no conflict of interest and nothing to disclose

Acknowledgments

This work was supported by grants from the Deutsche Forschungsgemeinschaft (AM 103/31-1;IG 18/20-1) and the Wellcome Trust (D.J.B. 110044/Z/15/Z). We thank the UKE research animal facility, in particular Gudrun Arndt and Nicole Lüder, for their excellent services. Moreover, we express our gratitude to Bettina Herde, Olga Winter, and Lana Rosenthal for technical assistance.

Author contributions: **Gretl Hendrickx**: Conceptualization; data curation; formal analysis; investigation; methodology; supervision; validation; visualization; writing-original draft; writing-review and editing. **Verena Fischer**: Investigation; validation. **Astrid Liedert**: Investigation; validation. **Simon von Kroge**: Investigation; validation. **Melanie Haffner-Luntzer**: Investigation; validation. **Laura Brylka**: Investigation; validation. **Eva Pawlus**: Investigation; validation. **Michaela Schweizer**: Investigation; resources; validation. **Timur Yorgan**: Formal analysis; investigation; validation. **Anke Baranowsky**: Investigation; validation. **Tim Rolvien**: Investigation; validation. **Mona Neven**: Investigation; validation. **Udo Schumacher**: Conceptualization; methodology. **David Beech**: Funding acquisition; methodology; resources. **Michael Amling**: Conceptualization; data curation; formal analysis; funding acquisition; methodology; project administration; resources; supervision; visualization; writing-original draft; writing-review and editing. **Anita Ignatius**: Conceptualization; data curation; formal analysis; funding acquisition; methodology; project administration; resources; supervision; visualization; writing-original draft; writing-review and editing. **Thorsten Schinke**: Conceptualization; data curation; formal analysis; methodology; project administration; resources; supervision; visualization; writing-original draft; writing-review and editing. Open access funding enabled and organized by Projekt DEAL.

Peer Review

The peer review history for this article is available at <https://publons.com/publon/10.1002/jbmr.4198>.

References

- Berendsen AD, Olsen BR. Bone development. *Bone*. 2015;80:14–8.
- Ferguson JW, Atit RP. A tale of two cities: the genetic mechanisms governing calvarial bone development. *Genesis*. 2019;57(1):e23248.
- Long F, Ornitz DM. Development of the endochondral skeleton. *Cold Spring Harb Perspect Biol*. 2013;5(1):a008334.
- Zaidi M. Skeletal remodeling in health and disease. *Nat Med*. 2007;13(7):791–801.
- Niedzwiedzki T, Filipowska J. Bone remodeling in the context of cellular and systemic regulation: The role of osteocytes and the nervous system. *J Mol Endocrinol*. 2015;55(2):R23–36.
- Ozcivici E, Luu YK, Adler B, et al. Mechanical signals as anabolic agents in bone. *Nat Rev Rheumatol*. 2010;6(1):50–9.
- Papachroni KK, Karatzas DN, Papavassiliou KA, Basdra EK, Papavassiliou AG. Mechanotransduction in osteoblast regulation and bone disease. *Trends Mol Med*. 2009;15(5):208–16.
- Vico L, Hargens A. Skeletal changes during and after spaceflight. *Nat Rev Rheumatol*. 2018;14(4):229–45.
- Dallas SL, Prideaux M, Bonewald LF. The osteocyte: an endocrine cell . . . and more. *Endocr Rev*. 2013;34(5):658–90.
- Tatsumi S, Ishii K, Amizuka N, et al. Targeted ablation of osteocytes induces osteoporosis with defective mechanotransduction. *Cell Metab*. 2007;5(6):464–75.
- Vining KH, Mooney DJ. Mechanical forces direct stem cell behaviour in development and regeneration. *Nat Rev Mol Cell Biol*. 2017;18(12):728–42.
- Gao J, Williams JL, Roan E. Multiscale modeling of growth plate cartilage mechanobiology. *Biomech Model Mechanobiol*. 2017;16(2):667–79.
- Kronenberg HM. Developmental regulation of the growth plate. *Nature*. 2003;423(6937):332–6.
- Michigami T. Regulatory mechanisms for the development of growth plate cartilage. *Cell Mol Life Sci*. 2013;70(22):4213–21.
- Aghajanian P, Mohan S. The art of building bone: emerging role of chondrocyte-to-osteoblast transdifferentiation in endochondral ossification. *Bone Res*. 2018;6:19.
- Mizuhashi K, Ono W, Matsushita Y, et al. Resting zone of the growth plate houses a unique class of skeletal stem cells. *Nature*. 2018;563(7730):254–8.
- Coste B, Mathur J, Schmidt M, et al. *Piezo1* and *Piezo2* are essential components of distinct mechanically activated cation channels. *Science*. 2010;330(6000):55–60.
- Ge J, Li W, Zhao Q, et al. Architecture of the mammalian mechanosensitive *Piezo1* channel. *Nature*. 2015;527(7576):64–9.
- Ridone P, Vassalli M, Martinac B. *Piezo1* mechanosensitive channels: what are they and why are they important. *Biophys Rev*. 2019;11(5):795–805.
- Wang L, Zhou H, Zhang M, et al. Structure and mechanogating of the mammalian tactile channel *PIEZO2*. *Nature*. 2019;573(7773):225–9.
- Gudipaty SA, Lindblom J, Loftus PD, et al. Mechanical stretch triggers rapid epithelial cell division through *Piezo1*. *Nature*. 2017;543(7643):118–21.
- Li J, Hou B, Tumova S, et al. *Piezo1* integration of vascular architecture with physiological force. *Nature*. 2014;515(7526):279–82.
- Solis AG, Bielecki P, Steach HR, et al. Mechanosensation of cyclical force by *PIEZO1* is essential for innate immunity. *Nature*. 2019;573(7772):69–74.
- Nonomura K, Woo SH, Chang RB, et al. *Piezo2* senses airway stretch and mediates lung inflation-induced apnoea. *Nature*. 2017;541(7636):176–81.
- Ranade SS, Woo SH, Dubin AE, et al. *Piezo2* is the major transducer of mechanical forces for touch sensation in mice. *Nature*. 2014;516(7529):121–5.
- Woo SH, Ranade S, Weyer AD, et al. *Piezo2* is required for Merkel-cell mechanotransduction. *Nature*. 2014;509(7502):622–6.

27. Albuissou J, Murthy SE, Bandell M, et al. Dehydrated hereditary stomatocytosis linked to gain-of-function mutations in mechanically activated PIEZO1 ion channels. *Nat Commun.* 2013;4:1884.
28. Andolfo I, Alper SL, De Franceschi L, et al. Multiple clinical forms of dehydrated hereditary stomatocytosis arise from mutations in PIEZO1. *Blood.* 2013;121(19):3925–35.
29. Zarychanski R, Schulz VP, Houston BL, et al. Mutations in the mechanotransduction protein PIEZO1 are associated with hereditary xerocytosis. *Blood.* 2012;120(9):1908–15.
30. Coste B, Houge G, Murray MF, et al. Gain-of-function mutations in the mechanically activated ion channel PIEZO2 cause a subtype of distal arthrogryposis. *Proc Natl Acad Sci U S A.* 2013;110(12):4667–72.
31. McMillin MJ, Beck AE, Chong JX, et al. Mutations in PIEZO2 cause Gordon syndrome, Marden-Walker syndrome, and distal arthrogryposis type 5. *Am J Hum Genet.* 2014;94(5):734–44.
32. Morris JA, Kemp JP, Youlten SE, et al. An atlas of genetic influences on osteoporosis in humans and mice. *Nat Genet.* 2019;51(2):258–66.
33. Sun W, Chi S, Li Y, et al. The mechanosensitive Piezo1 channel is required for bone formation. *Elife.* 2019;8:e47454.
34. Li X, Han L, Nookaew I, et al. Stimulation of Piezo1 by mechanical signals promotes bone anabolism. *Elife.* 2019;8:e49631.
35. Wang L, You X, Lotinun S, Zhang L, Wu N, Zou W. Mechanical sensing protein PIEZO1 regulates bone homeostasis via osteoblast-osteoclast crosstalk. *Nat Commun.* 2020;11(1):282.
36. Zhou T, Gao B, Fan Y, et al. Piezo1/2 mediate mechanotransduction essential for bone formation through concerted activation of NFAT-YAP1-ss-catenin. *Elife.* 2020;9:e52779.
37. Keller J, Catala-Lehnen P, Huebner AK, et al. Calcitonin controls bone formation by inhibiting the release of sphingosine 1-phosphate from osteoclasts. *Nat Commun.* 2014;5:5215.
38. Lu Y, Xie Y, Zhang S, Dusevich V, Bonewald LF, Feng JQ. DMP1-targeted Cre expression in odontoblasts and osteocytes. *J Dent Res.* 2007;86(4):320–5.
39. Rauch A, Seitz S, Baschant U, et al. Glucocorticoids suppress bone formation by attenuating osteoblast differentiation via the monomeric glucocorticoid receptor. *Cell Metab.* 2010;11(6):517–31.
40. Clausen BE, Burkhardt C, Reith W, Renkawitz R, Forster I. Conditional gene targeting in macrophages and granulocytes using LysMcre mice. *Transgenic Res.* 1999;8(4):265–77.
41. Ovchinnikov DA, Deng JM, Ogunrinu G, Behringer RR. Col2a1-directed expression of Cre recombinase in differentiating chondrocytes in transgenic mice. *Genesis.* 2000;26(2):145–6.
42. Liedert A, Mattausch L, Rontgen V, et al. Midkine-deficiency increases the anabolic response of cortical bone to mechanical loading. *Bone.* 2011;48(4):945–51.
43. Rapp AE, Kroner J, Baur S, et al. Analgesia via blockade of NGF/TrkA signaling does not influence fracture healing in mice. *J Orthop Res.* 2015;33(8):1235–41.
44. Schinke T, Schilling AF, Baranowsky A, et al. Impaired gastric acidification negatively affects calcium homeostasis and bone mass. *Nat Med.* 2009;15(6):674–81.
45. Pohl S, Angermann A, Jeschke A, et al. The lysosomal protein arylsulfatase B is a key enzyme involved in skeletal turnover. *J Bone Miner Res.* 2018;33(12):2186–201.
46. Dempster DW, Compston JE, Drezner MK, et al. Standardized nomenclature, symbols, and units for bone histomorphometry: a 2012 update of the report of the ASBMR Histomorphometry nomenclature committee. *J Bone Miner Res.* 2013;28(1):2–17.
47. Milovanovic P, Zimmermann EA, Hahn M, et al. Osteocytic canalicular networks: morphological implications for altered mechanosensitivity. *ACS Nano.* 2013;7(9):7542–51.
48. Sugimoto A, Miyazaki A, Kawarabayashi K, et al. Piezo type mechanosensitive ion channel component 1 functions as a regulator of the cell fate determination of mesenchymal stem cells. *Sci Rep.* 2017;7(1):17696.
49. Blaber EA, Dvorochkin N, Lee C, et al. Microgravity induces pelvic bone loss through osteoclastic activity, osteocytic osteolysis, and osteoblastic cell cycle inhibition by CDKN1a/p21. *PLoS One.* 2013;8(4):e61372.
50. Dy P, Wang W, Bhattaram P, et al. Sox9 directs hypertrophic maturation and blocks osteoblast differentiation of growth plate chondrocytes. *Dev Cell.* 2012;22(3):597–609.
51. Zhang P, Liegeois NJ, Wong C, et al. Altered cell differentiation and proliferation in mice lacking p57KIP2 indicates a role in Beckwith-Wiedemann syndrome. *Nature.* 1997;387(6629):151–8.
52. Laplante M, Sabatini DM. mTOR signaling in growth control and disease. *Cell.* 2012;149(2):274–93.
53. Csukas F, Duran I, Barad M, et al. The PTH/PTHrP-SIK3 pathway affects skeletogenesis through altered mTOR signaling. *Sci Transl Med.* 2018;10(459):eaat9356.
54. Gerber HP, Vu TH, Ryan AM, Kowalski J, Werb Z, Ferrara N. VEGF couples hypertrophic cartilage remodeling, ossification and angiogenesis during endochondral bone formation. *Nat Med.* 1999;5(6):623–8.
55. Yao Y, Wang Y. ATDC5: an excellent in vitro model cell line for skeletal development. *J Cell Biochem.* 2013;114(6):1223–9.
56. Ono N, Ono W, Nagasawa T, Kronenberg HM. A subset of chondrogenic cells provides early mesenchymal progenitors in growing bones. *Nat Cell Biol.* 2014;16(12):1157–67.
57. Yang L, Tsang KY, Tang HC, Chan D, Cheah KS. Hypertrophic chondrocytes can become osteoblasts and osteocytes in endochondral bone formation. *Proc Natl Acad Sci U S A.* 2014;111(33):12097–102.
58. Takarada T, Hinoi E, Nakazato R, et al. An analysis of skeletal development in osteoblast-specific and chondrocyte-specific runt-related transcription factor-2 (Runx2) knockout mice. *J Bone Miner Res.* 2013;28(10):2064–9.
59. Takeda S, Bonnamy JP, Owen MJ, Ducey P, Karsenty G. Continuous expression of Cbfa1 in nonhypertrophic chondrocytes uncovers its ability to induce hypertrophic chondrocyte differentiation and partially rescues Cbfa1-deficient mice. *Genes Dev.* 2001;15(4):467–81.
60. Haelterman N, Lim J. Sensing the load. *Elife.* 2019;8:e50210.
61. Luther J, Yorgan TA, Rolvien T, et al. Wnt1 is an Lrp5-independent bone-anabolic Wnt ligand. *Sci Transl Med.* 2018;10(466):eaau7137.
62. Bai WY, Wang L, Ying ZM, et al. Identification of PIEZO1 polymorphisms for human bone mineral density. *Bone.* 2020;133:115247.
63. Morley LC, Beech DJ, Walker JJ, Simpson NAB. Emerging concepts of shear stress in placental development and function. *Mol Hum Reprod.* 2019;25(6):329–39.
64. Wang Y, Chi S, Guo H, et al. A lever-like transduction pathway for long-distance chemical- and mechano-gating of the mechanosensitive Piezo1 channel. *Nat Commun.* 2018;9(1):1300.